Sagittarius A* and Low Luminosity Accreting Sources

EWAS 2017, 26-30 June 2017 * Prague, Czech Republic; No. 1387

S12f – Accretion Blasck holes at their extremes

Andreas Eckart

I.Physikalisches Institut der Universität zu Köln

Max-Planck-Institut für Radioastronomie, Bonn

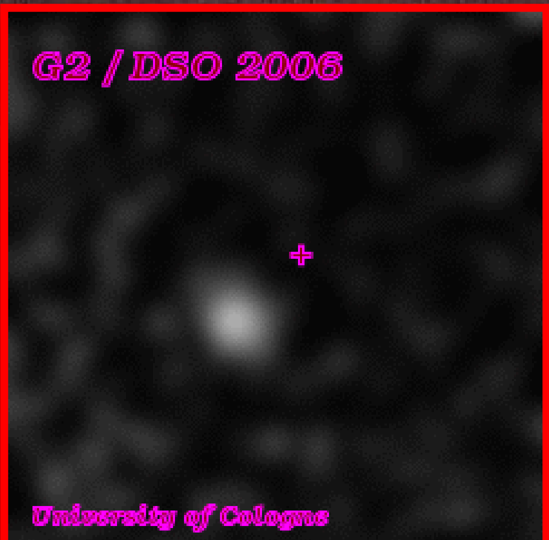

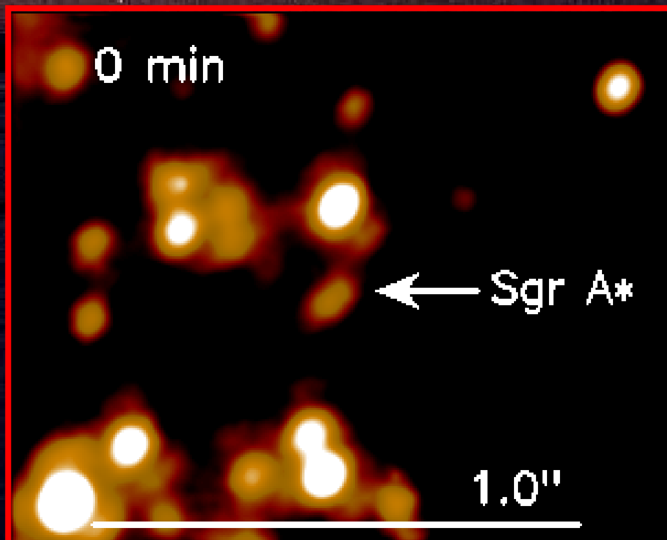

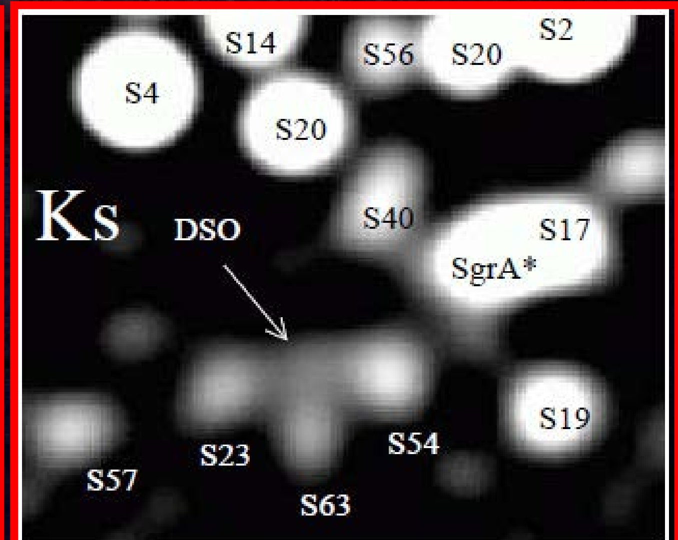

Plan

- Accretion as the origin of luminosity
- Comparing SgrA* to LLAGN:
  Radio sources in the optical diagnostic diagram.
- SgrA* as a Low Luminosity (aktive) Source
- Radio domain: variability / spectral index
- Submillimeter domain (?)
- Mid/Near-infrared domain
- Optical/ UV (?)
- X-Ray domain
- γ-Ray domain (?)

(?) = not accessable, no sufficient angular resolution or sensitivity

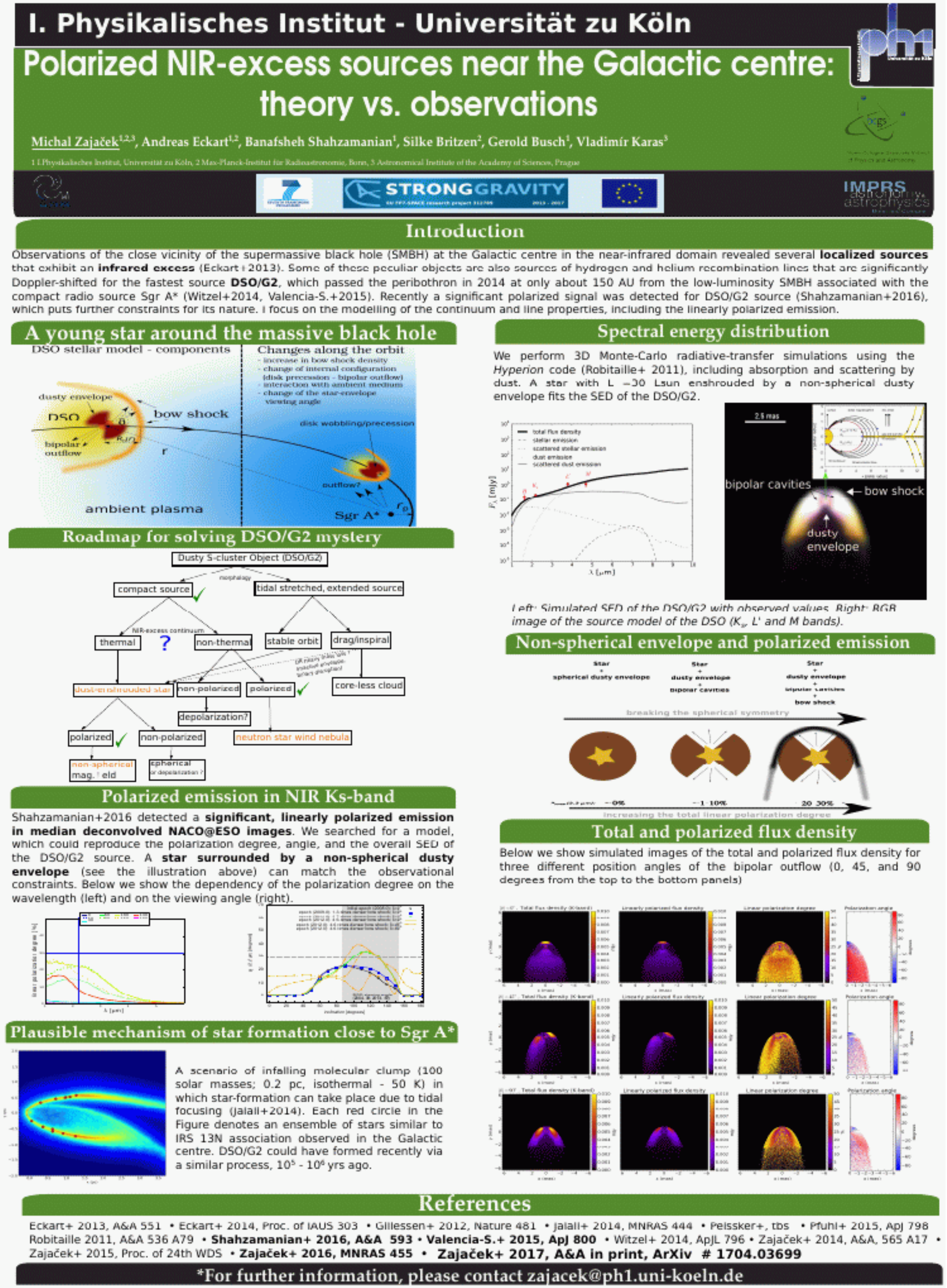

Please see also S12 poster by

Michal Zajacek

Polarized NIR-excess sources near the Galactic centre: Theory vs. Observations

Accretion as
Origin of the Luminosity

Accretion onto SMBs

CASE 1: low accretion rate
high opacity

$$\dot{M}/\dot{M}_E \lesssim 0.1$$

thin accretion disk compared to diameter
efficiency: $\eta \approx 0.1$

CASE 0:
plus advection dominated accretion for LLAGN

$\dot{M}/\dot{M}_E$

SgrA*

X-ray
UV

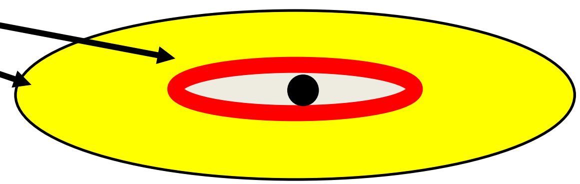

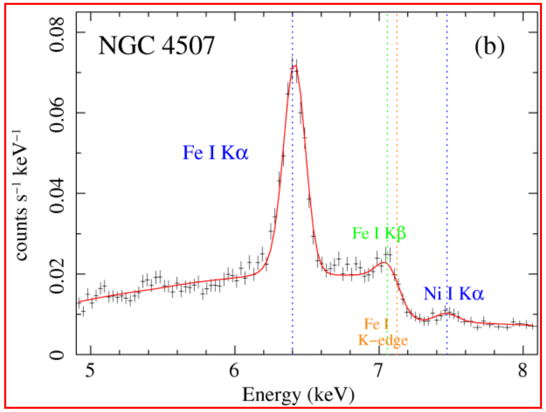

Suzaku data

CASE 2: high accretion rate
radiation heats disk
disk inflates and cools
at larger radii, i.e.
radiation becomes
inefficient.

$$\dot{M}/\dot{M}_E \gg 1$$

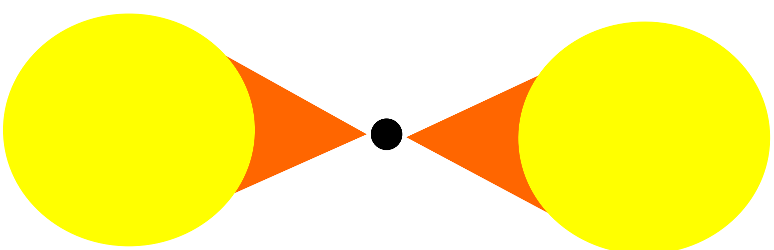

looks like a
10**4 K
young star

Accretion onto SMBs

CASE 0:

plus advection dominated accretion for LLAGN

$\dot{M} / \dot{M}_{\rm E}$

SgrA*

X-ray

UV

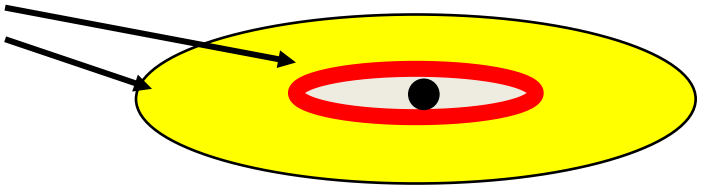

Thin disks are possible but
advection dominated accretion may be
a dominant operation mode for these sources

The proposed unification scheme of Falcke et al. (2004) for accreting black holes in the mass and accretion rate plane. The X-axis denotes the black hole mass and the Y -axis the accretion power. For stellar black holes it coincides with the two normal black hole states.
For the AGN zoo we include low-luminosity AGN (LLAGN), radio galaxies (RG), low ionization emission region sources (LINER), Seyferts, and quasars.

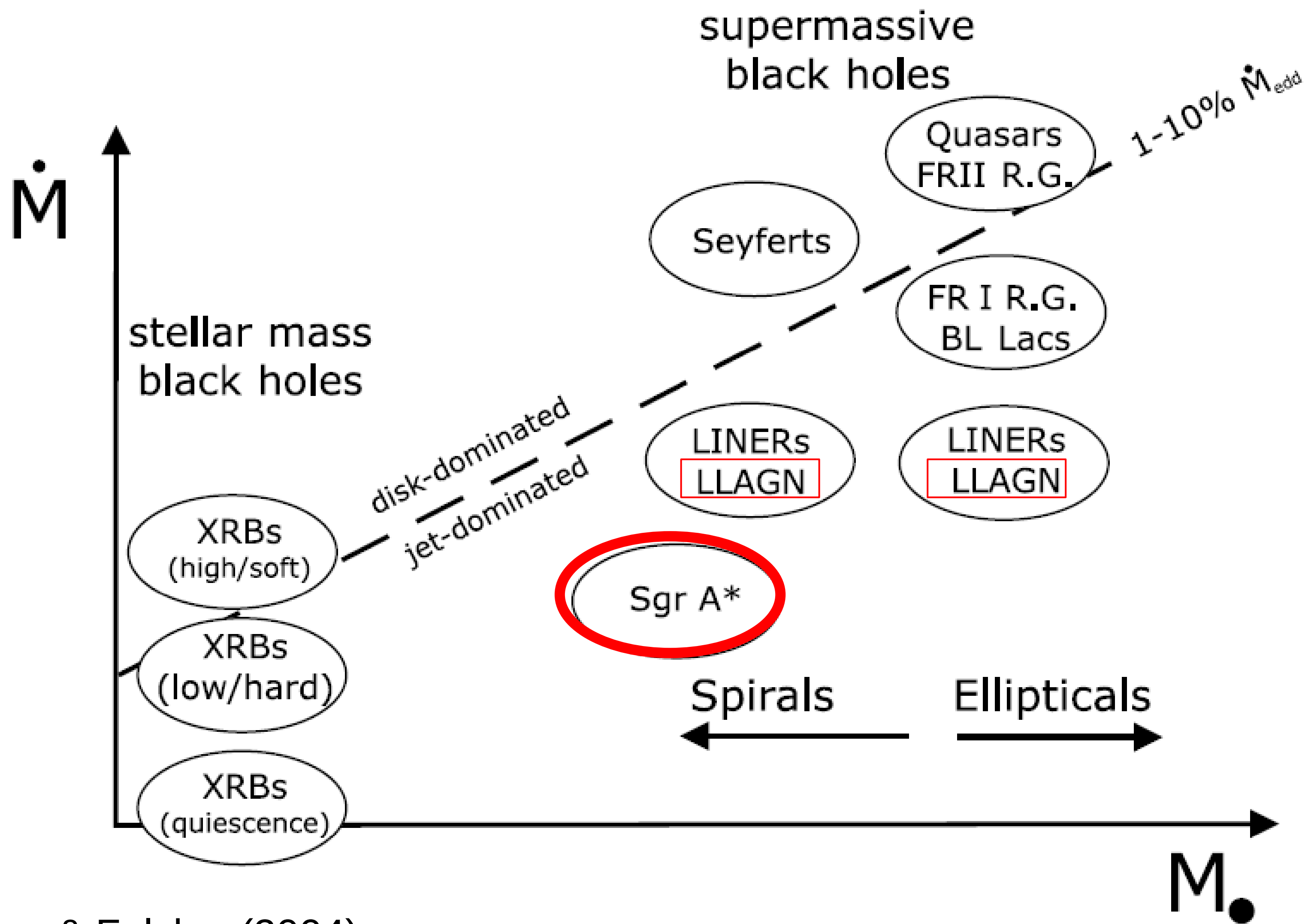

Körding & Falcke (2004)

Demographics of activity in nearby galaxies.

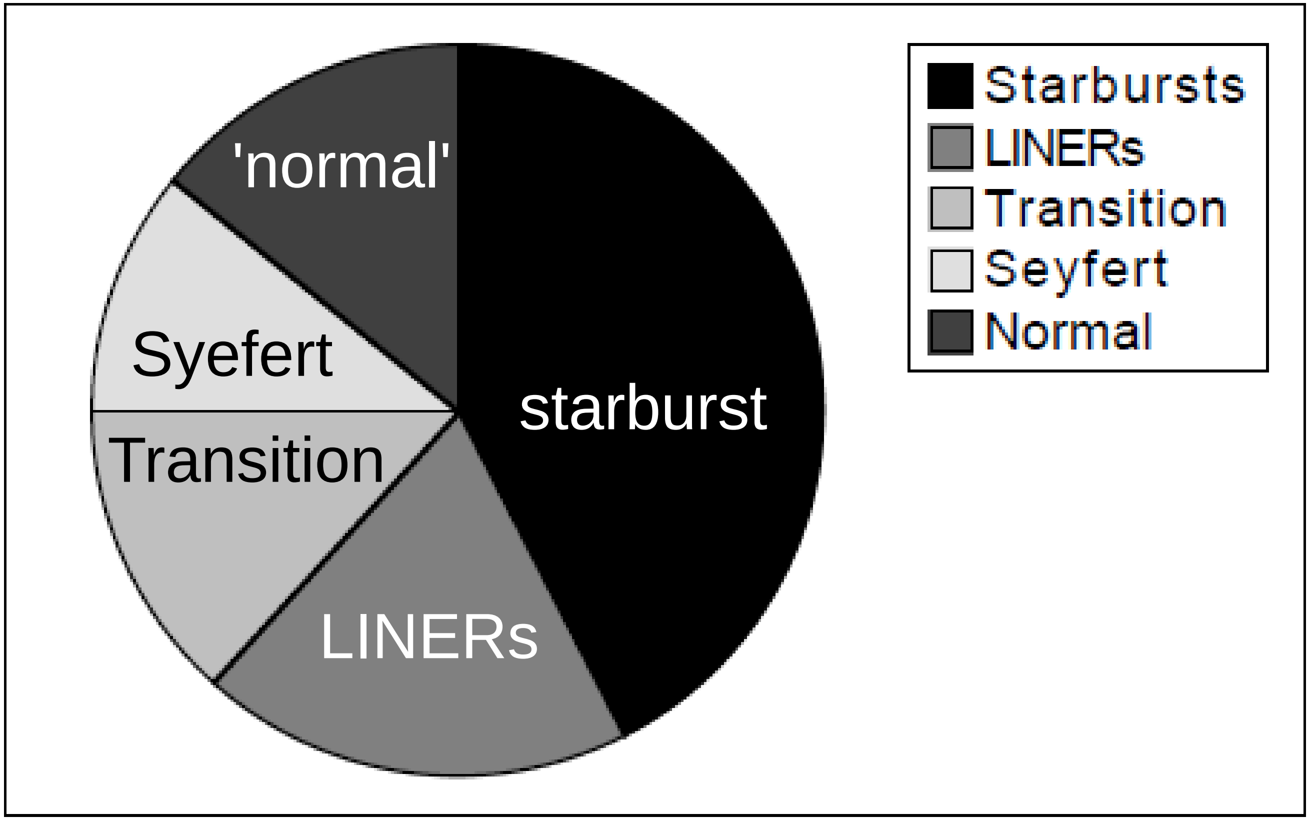

Ptak 2000

Low-luminosity AGN (with Lx < 10^42 ergs s^−1) far outnumber ordinary AGN, and are therefore perhaps more relevant to our understanding of AGN phenomena and the relationship between AGN and host galaxies. Many normal galaxies harbor LINER and starburst nuclei, which, together with LLAGN, are a class of “low-activity” galaxies that have a number of surprisingly similar X-ray characteristics, despite their heterogenous optical classification. This strongly supports the hypothesis of an AGN-starburst connection.

MBH scaling relation for spiral galaxies, spheroids, ellipticals

Koliopanos et al (2017) find that all LLAGN in their list have low-mass central black holes with log MBH/M☉≈6.5 on average (closer to spirals, below ellipticals ?).

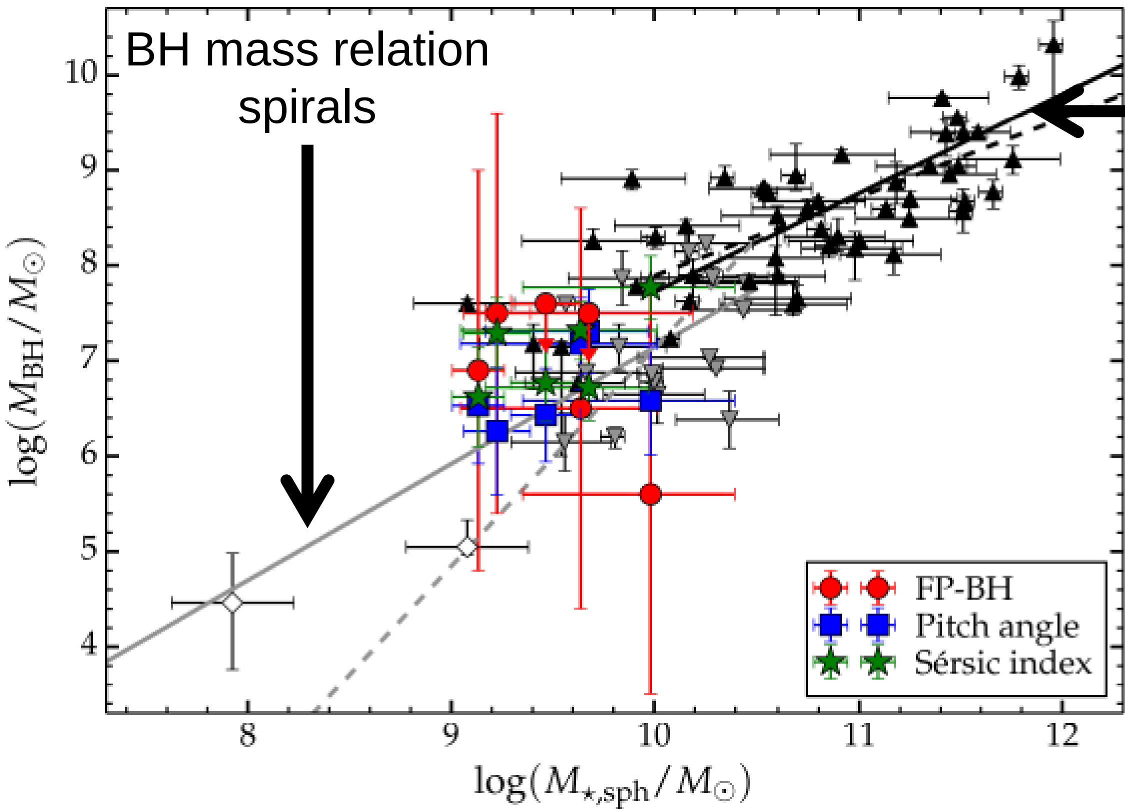

BH mass relation ellipticals

Koliopanos et al. 2017

Low Surface brightness AGN tend to have BH masses below the standard relations for spirals and ellipticals.

Subramanian et al. 2016

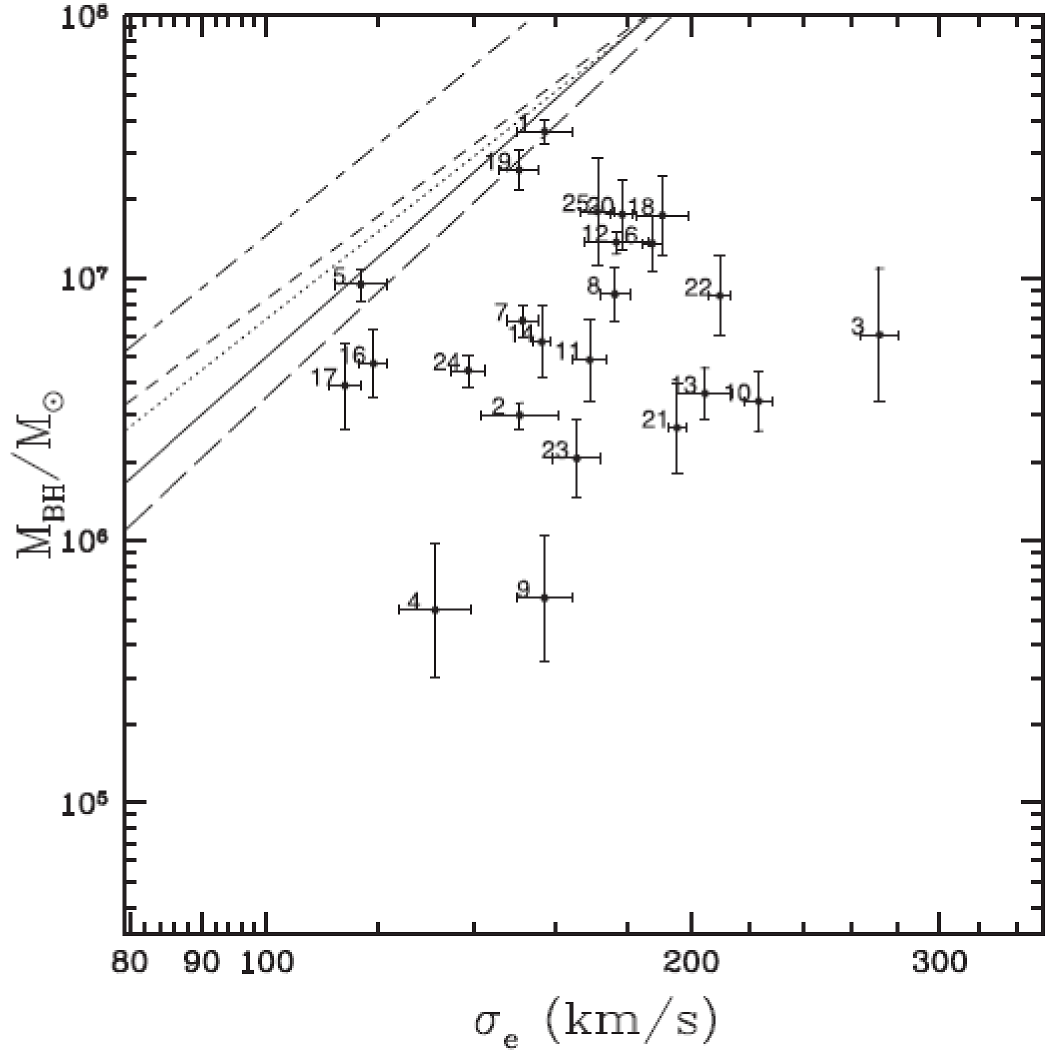

The M–σe plot with broad line AGN candidates. The linear regression lines given by Tremaine et al. (2002), Ferrarese & Merritt (2000), Gültekin et al. (2009) and Kormendy & Ho (2013) relation for classical bulges/elliptical galaxies and (McConnell &Ma 2013) relation for late-type galaxies (dashed, solid, dotted short-long dashed and long-dashed lines, respectively) for MBH against σe are also shown.

Starformation and Blackhole Growth in Nearby QSOs

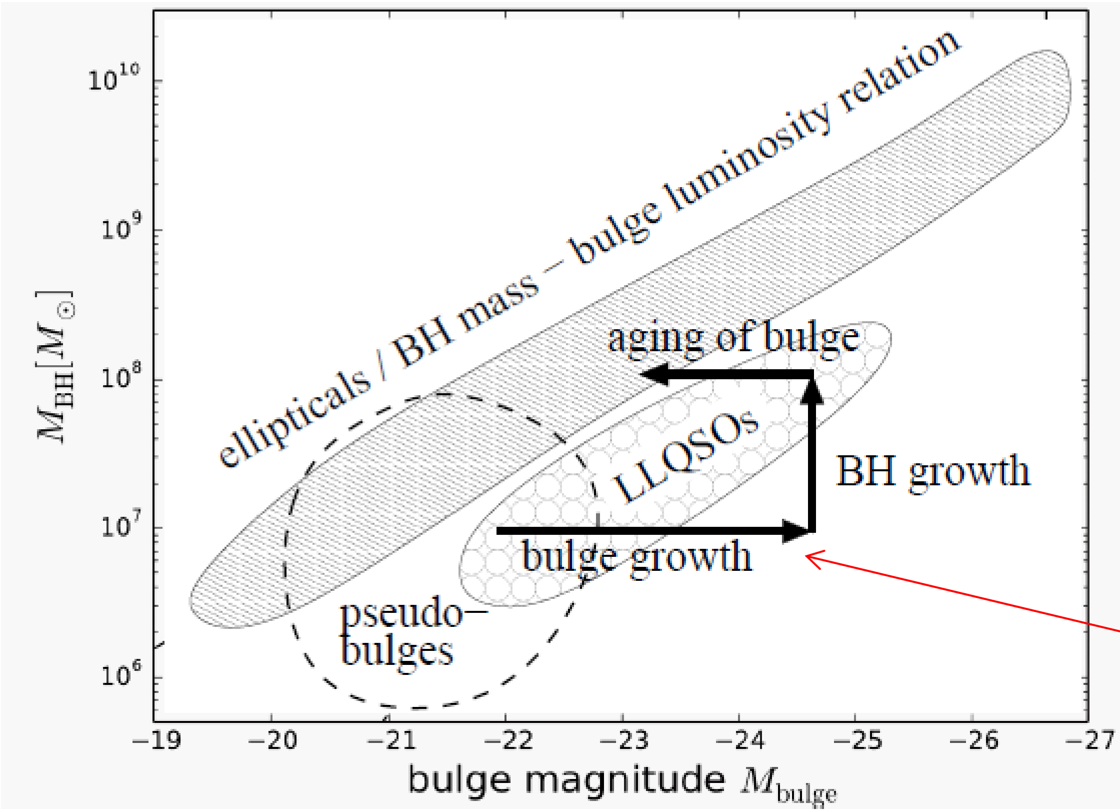

Bulge Luminosity Growth:
Conditions of Starformation
in Nuclei of Galaxies

Figure 2: A possible evolutionary scenario in the black hole mass - bulge luminosity diagram. Accretion of matter onto the central region results into enhanced star formation and black hole growth. Young stellar populations cause over-luminous bulges compared to inactive galaxies on the relation. Black hole growth and aging of the stellar populations then move the objects back onto the relation.

Busch et al. 2016

Comparing SgrA* to LLAGN

-

Radio sources in the optical diagnostic diagram.

Radio sources in the optical diagnostic diagram.

sea gull – PBT diagram

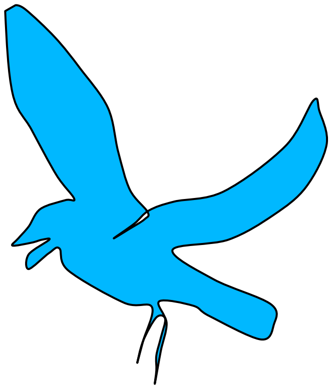

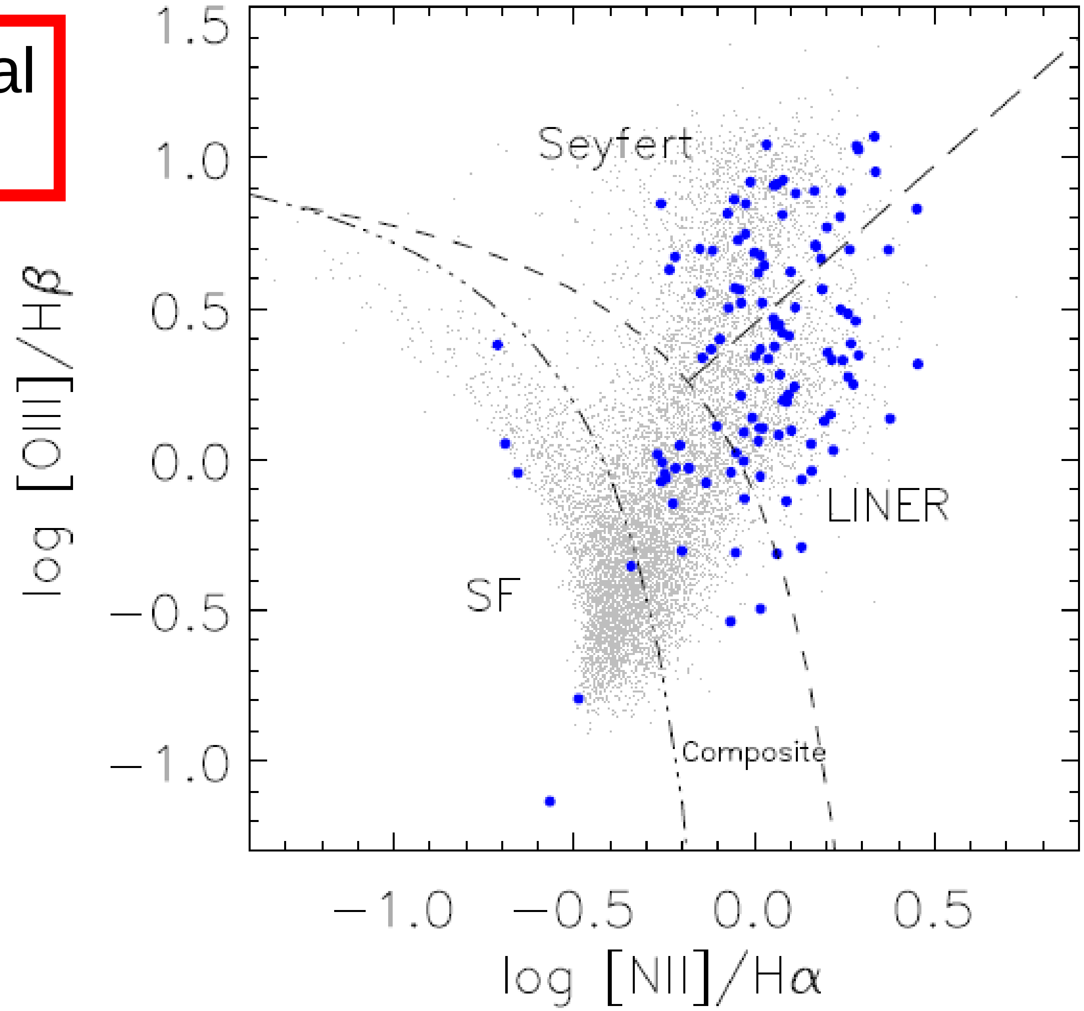

Vitale et al. 20012/15

[NII]-based diagnostic diagrams of the parent (gray) and Effelsberg (blue) samples. Demarcation lines were derived by Kewley et al. (2001; dashed) to set an upper limit for the position of starforming galaxies and by Kauffmann et al. (2003b; three-point dashed) to trace the observed lower left branch (purely star-forming galaxies) more closely. The dividing line between Seyferts and LINERs (long dashed) was set by Schawinski et al. (2007).

Radio spectral indices in the optical diagnostic diagram.

Red: flat/inverted
Blue: steep.

Radio emission only along the right wing of the sea gull

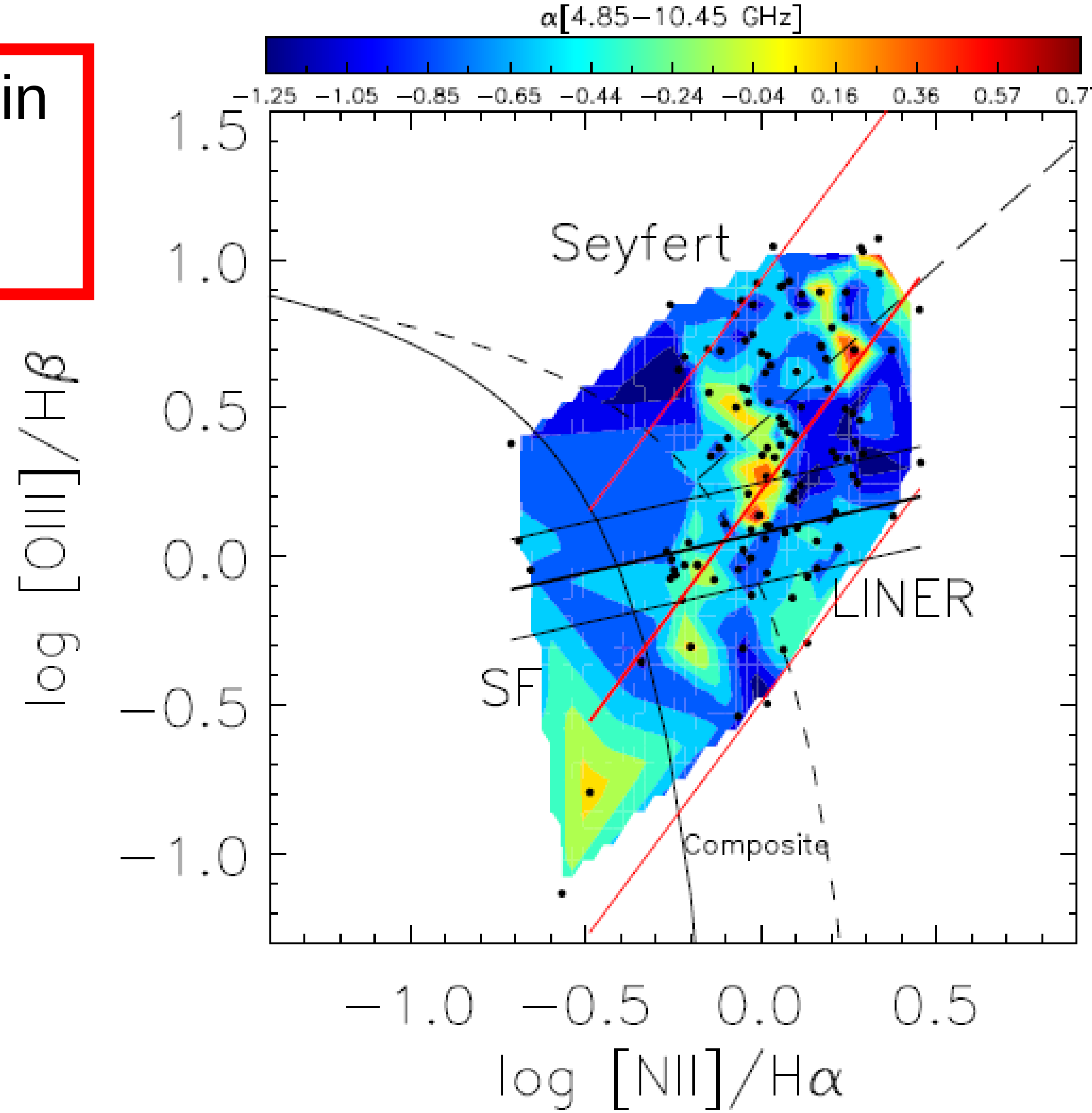

Vitale et al. 20012/15

Two-point spectral index distribution of the Effelsberg sample represented in the [NII] based diagnostic diagram. The color gradient indicates the spectral index values. Black dots correspond to sources positions in the diagram. Red thick lines are regression curves of the 15% most flat- and inverted-spectrum sources; black thick lines are regression curves of the steep-spectrum sources

Stellar Mass increase of Radio LLAGN in the optical diagnostic diagram.

Possible Evolution (Mass and/or Object) Of Radio LLAGN in the optical diagnostic diagram.

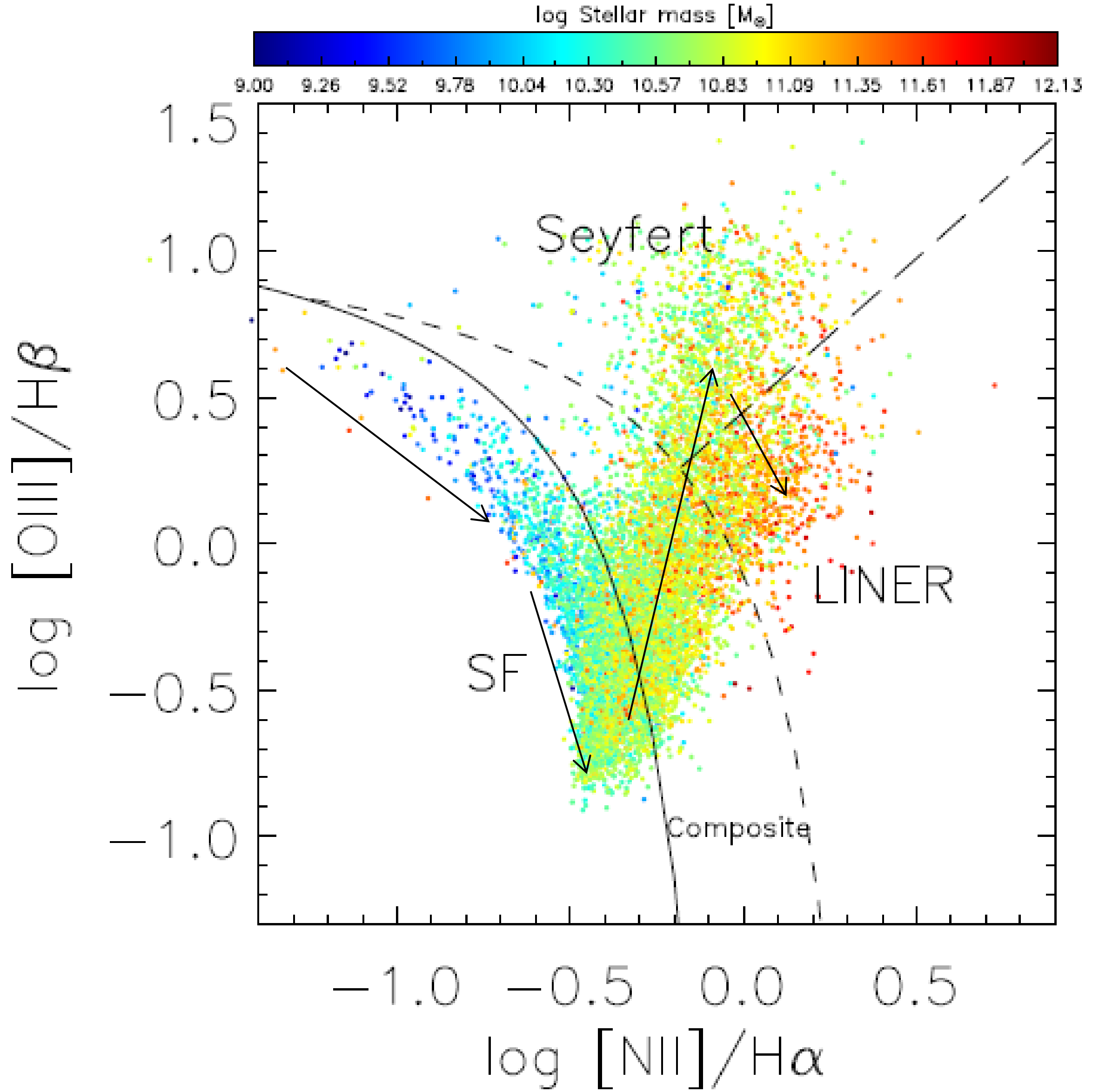

Vitale et al. 20012/15

SDSS-FIRST stellar mass distribution in the [NII]-based diagnostic diagram. The color bar indicates the stellar mass values from SDSS measurements, in solar units.

Radio sources in the optical diagnostic diagram.

For SgrA* region the optical line ratios are not available but …

based on stellar mass BH mass and radio activity SgrA* must be placed somewhere here:

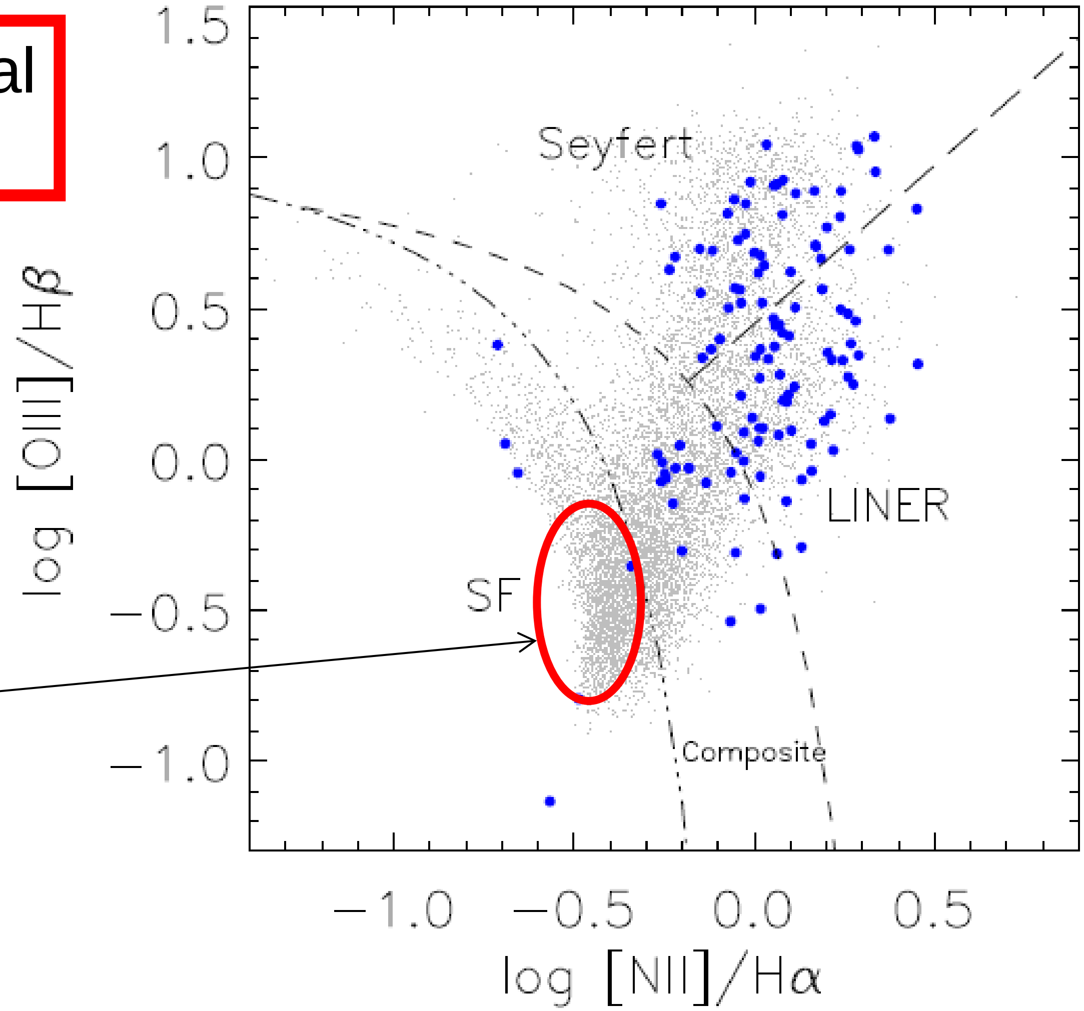

Vitale et al. 20012/15

[NII]-based diagnostic diagrams of the parent (gray) and Effelsberg (blue) samples. Demarcation lines were derived by Kewley et al. (2001; dashed) to set an upper limit for the position of starforming galaxies and by Kauffmann et al. (2003b; three-point dashed) to trace the observed lower left branch (purely star-forming galaxies) more closely. The dividing line between Seyferts and LINERs (long dashed) was set by Schawinski et al. (2007).

SgrA* as an extreme LLAGN

SgrA* as an extreme LLAGN Nucleus

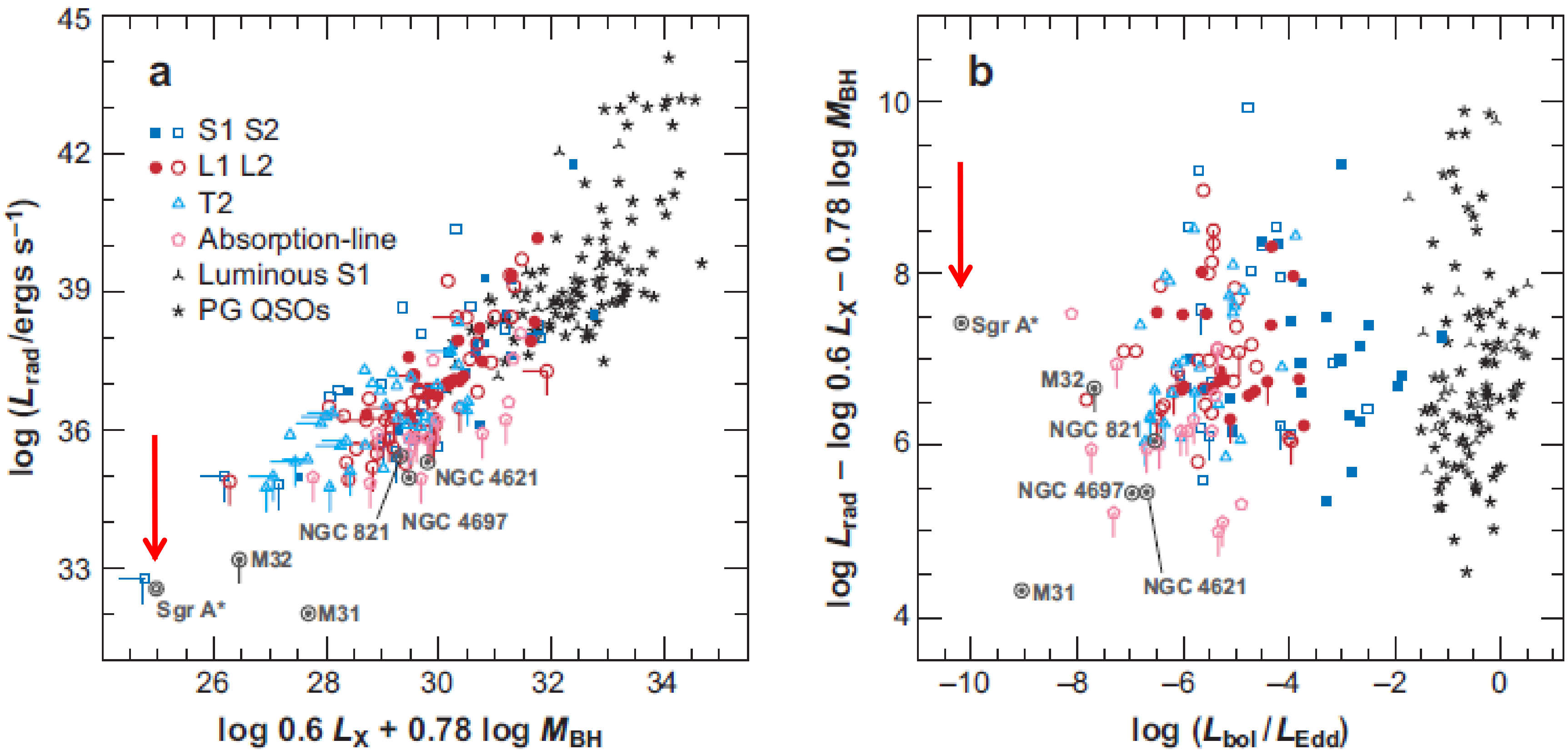

Ho 2008: Fundamental plane correlation among core radio luminosity, X-ray (a)luminosity, and BH mass. (*b*) Deviations from the fundamental plane as a function of Eddington ratio.

SgrA* is accreting in an advection dominated mode, else ist luminosity would be than 10^7 times higher

SgrA* and its Environment

Orbits of High Velocity Stars
in the Central Arcsecond

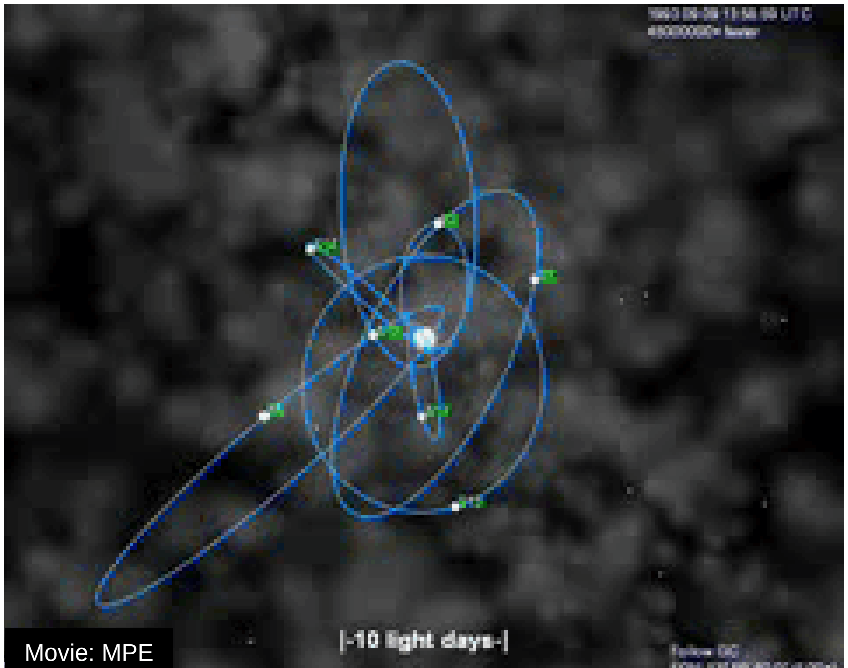

Eckart & Genzel 1996/1997 (first proper motions)
Eckart+2002 (S2 is bound; first elements)
Schödel+ 2002, 2003 (first detailed elements)
Ghez+ 2003 (detailed elements)
Eisenhauer+ 2005, Gillessen+ 2009
(improving orbital elements)
Rubilar & Eckart 2001, Sabha+ 2012, Zucker+2006
(exploring the relativistic character of orbits)

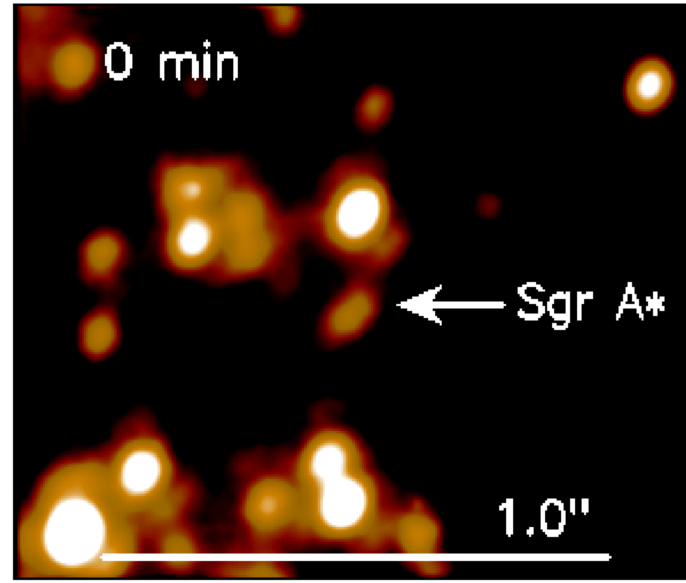

See also review by
Eckart et al. 20017 in
‘Foundations of Physics‘

~4.3 million solar masses
at a distance of
~8+-0.3 kpc

Accretion of winds onto SgrA*

Starvation?

NIR and X-ray observations as well as simulations suggest stellar winds contribute up to 10^-4 MSun/yr at Bondi radius (10^5 rS) (Krabbe+ 1995, Baganoff+ 2003)

At this accretrion rate SgrA* is 10^7 times under luminous (e.g. Shcherbakov & Baganoff 2010)

Accretion of gaseous clumps from the Galactic Centre Mini-spiral onto Milky Way's supermassive black hole ? (Karas, Vladimir; Kunneriath, Devaky; Czerny, Bozena; Rozanska, Agata; Adhikari, Tek P. ; 2016grg..conf...98K)

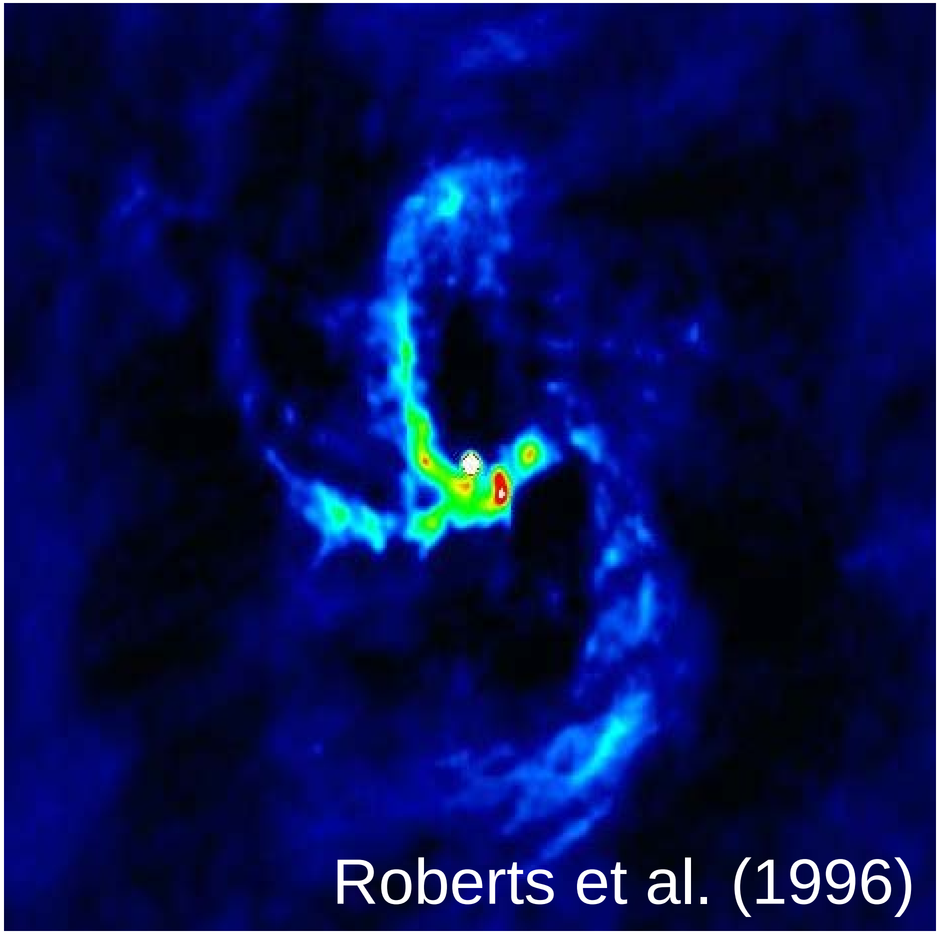

Flare Activity of SgrA*

Seeing the effect of ongoing accretion

Flare Emission from SgrA*

Recent work on SgrA* variability

Radio/sub-mm:

Mauerhan+2005, Marrone+2006/8,
Yusef-Zadeh+2006/8 and may others

X-ray:

Baganoff+2001/3, Porquet+2003/2008,
Eckart+2006/8, Ponti+2017 and several others

NIR:

Genzel+2003, Ghez+2004, Eckart+2006/9,
Hornstein+2007,Do+2009, and many others

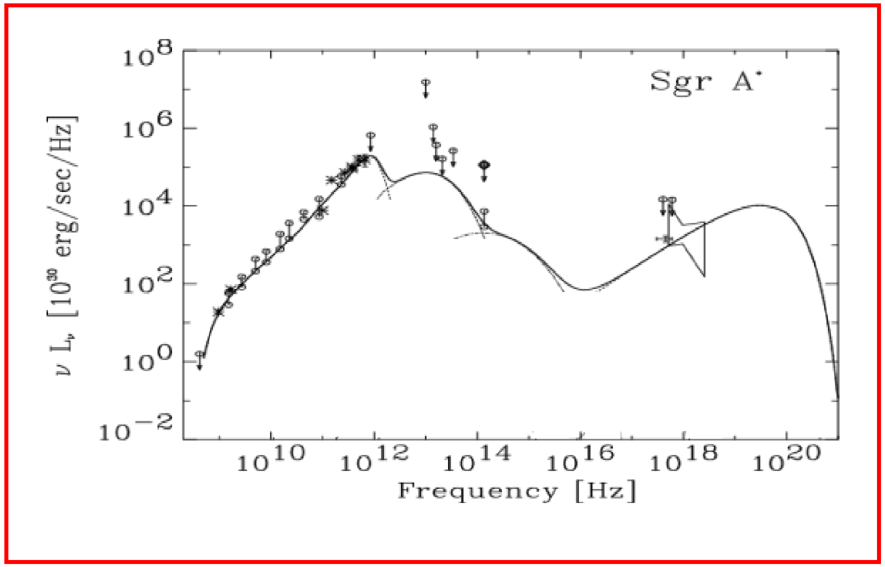

Multi frequency observing programs:

Genzel, Ghez, Yusef-Zadeh, Eckart and many others

Questions:

- What are the radiation mechanisms?
- How are the particles accelerated?
- (How) Are flux density variations at different wavelength connected to each other?

Flare Emission from SgrA*

Radio spectral Index +0.3

Optically thin synchrotron radiation

Optically thin synchrotron radiation or (much easier) SSC

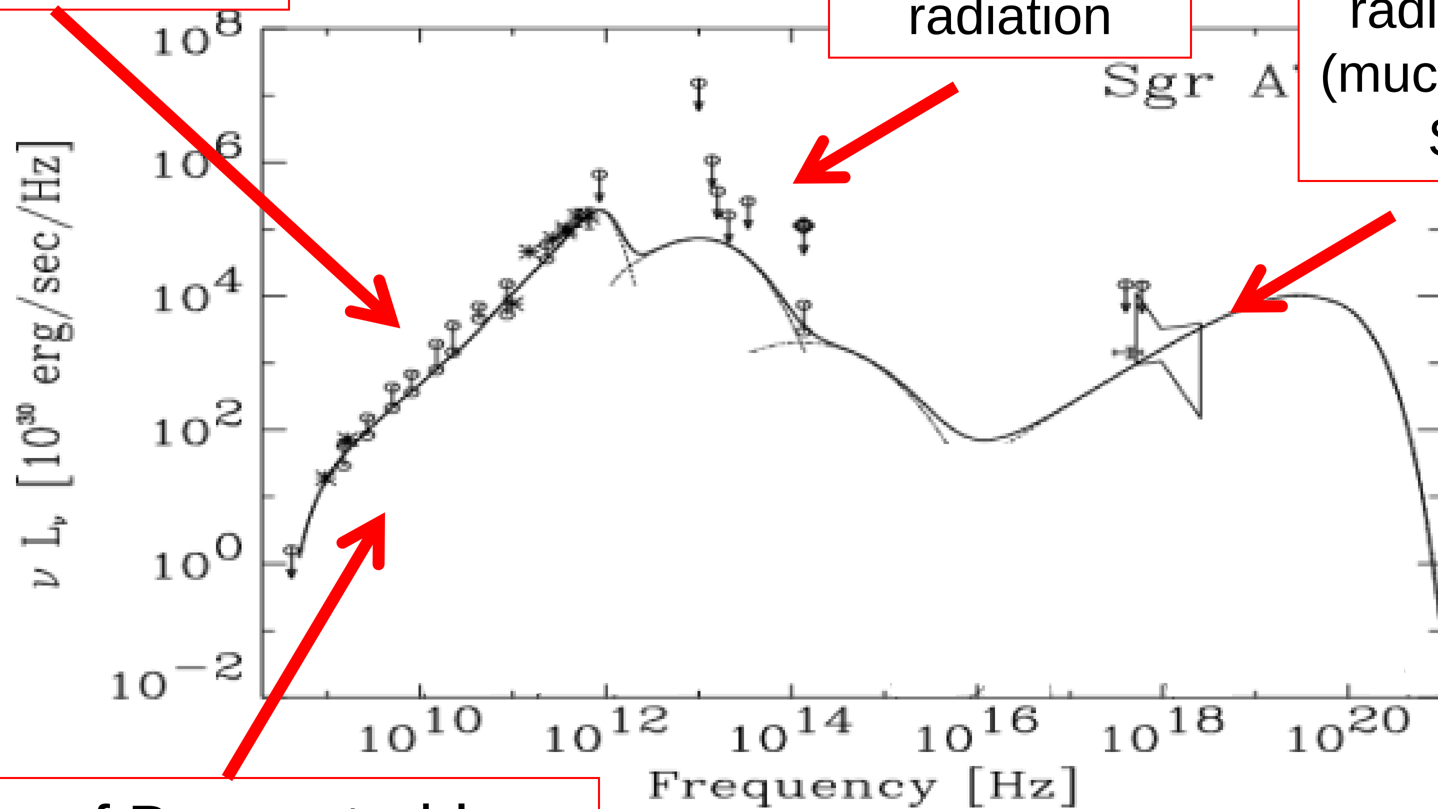

Mixture of Bremsstrahlung (Gyro-)synchrotron

Small contributions from 1“ extended Bremss. blob

Observations

SgrA* on 3 June 2008:
VLT L-band and APEX
sub-mm measurements

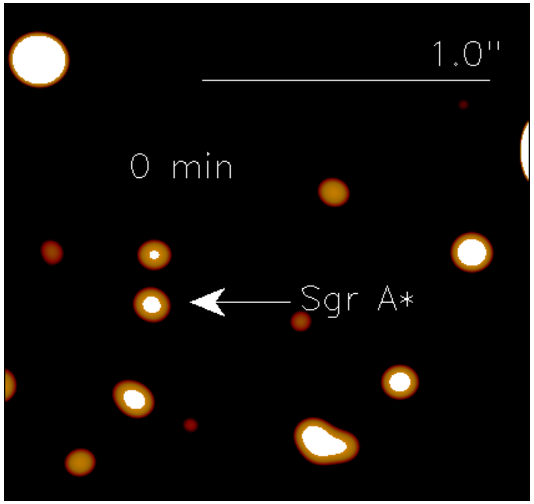

VLT 3.8um L-band

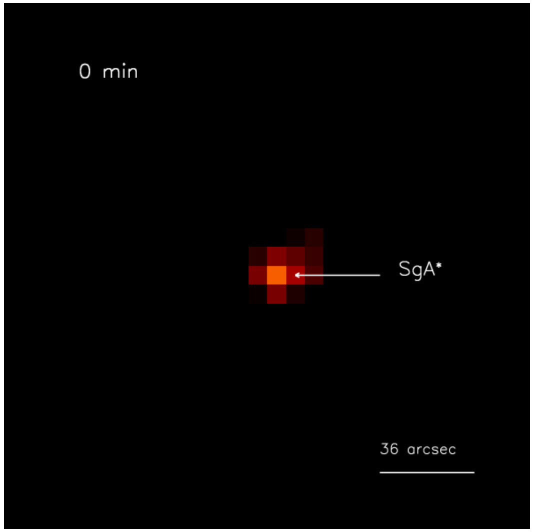

APEX 1.3 mm

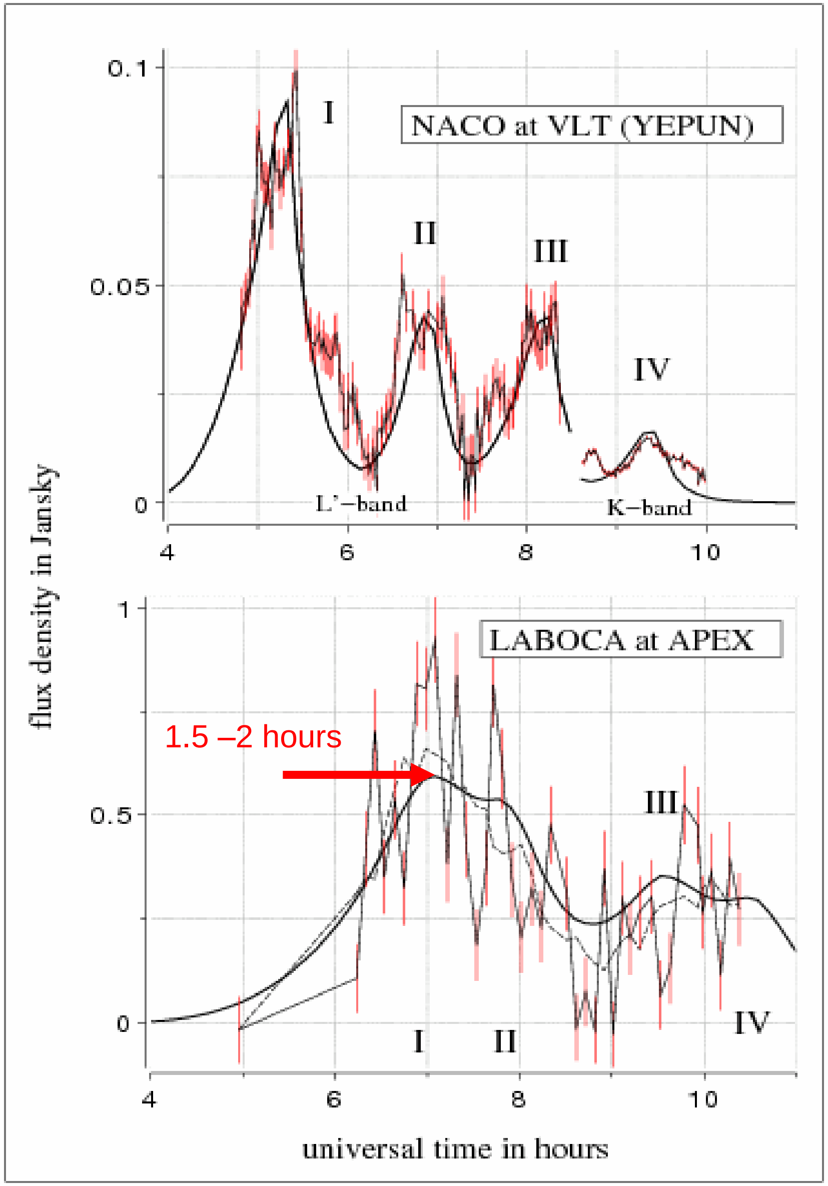

Eckart et al. 2008; A&A 492, 337
Garcia-Marin et al.2009

Simultaueous NIR/X-ray Flare emission 2004

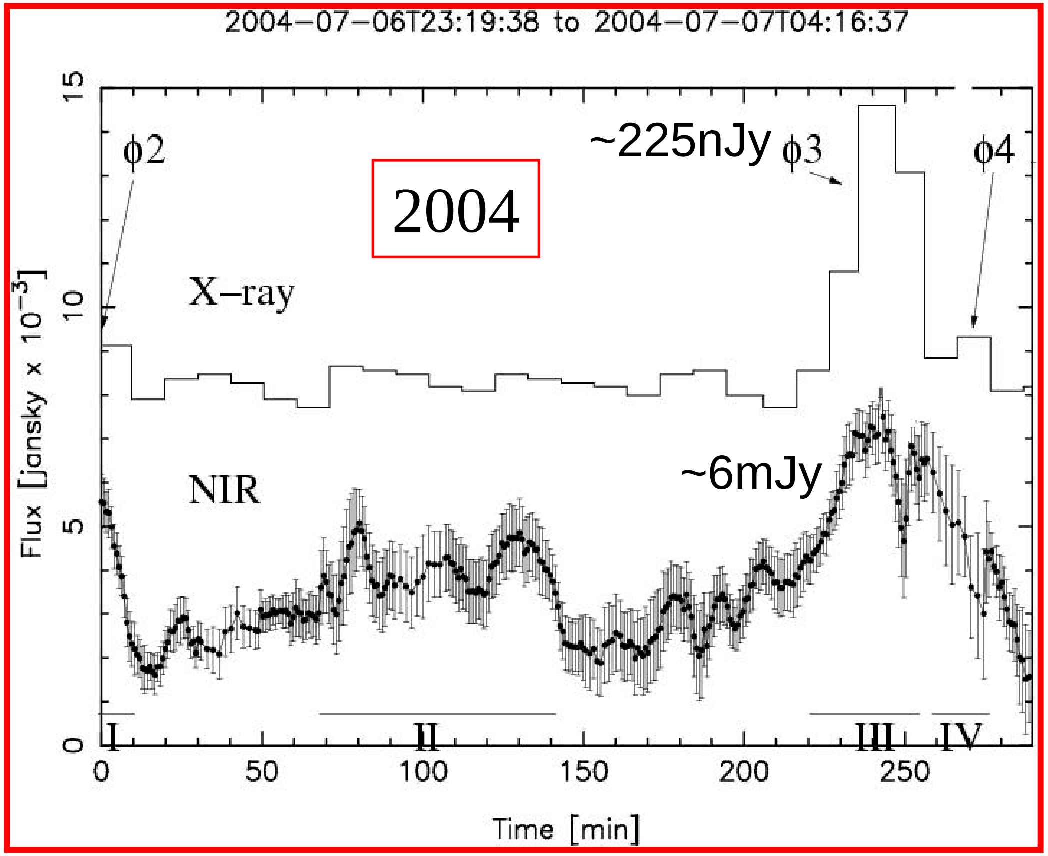

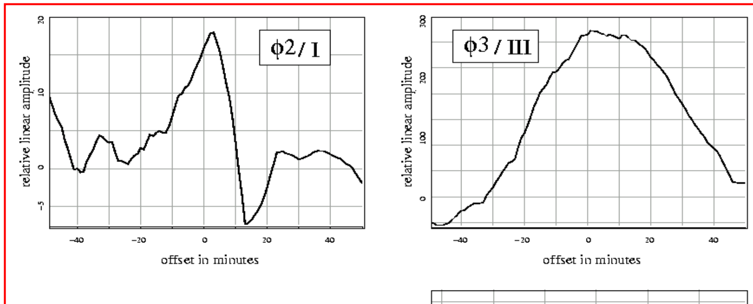

Time lags are less <10-15 minutes

NIR and X-ray flares are well correlated.

Flare emission originates from within <10mas form the position of SgrA*

First simultaneous NIR/X-ray detection

2003 data: Eckart, Baganoff, Morris, Bautz, Brandt, et al. 2004 A&A 427, 1

2004 data: Eckart, Morris, Baganoff, Bower, Marrone et al. 2006 A&A 450, 535

see also Yusef-Zadeh, et al. 2008, Marrone et al. 2008

Simultaueous NIR/X-ray Flare emission 2004

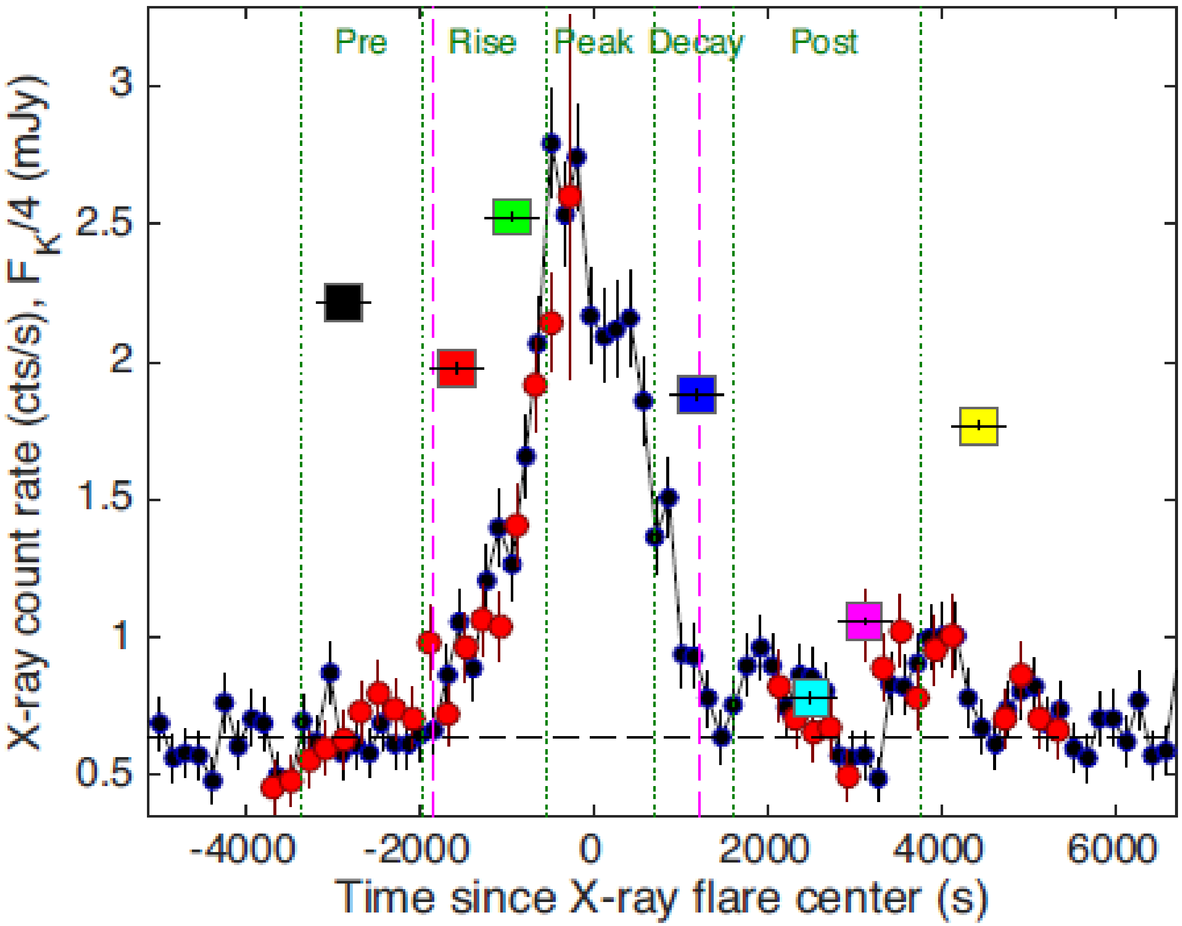

Ponti et al. 2017

Synchrotron versus SSC

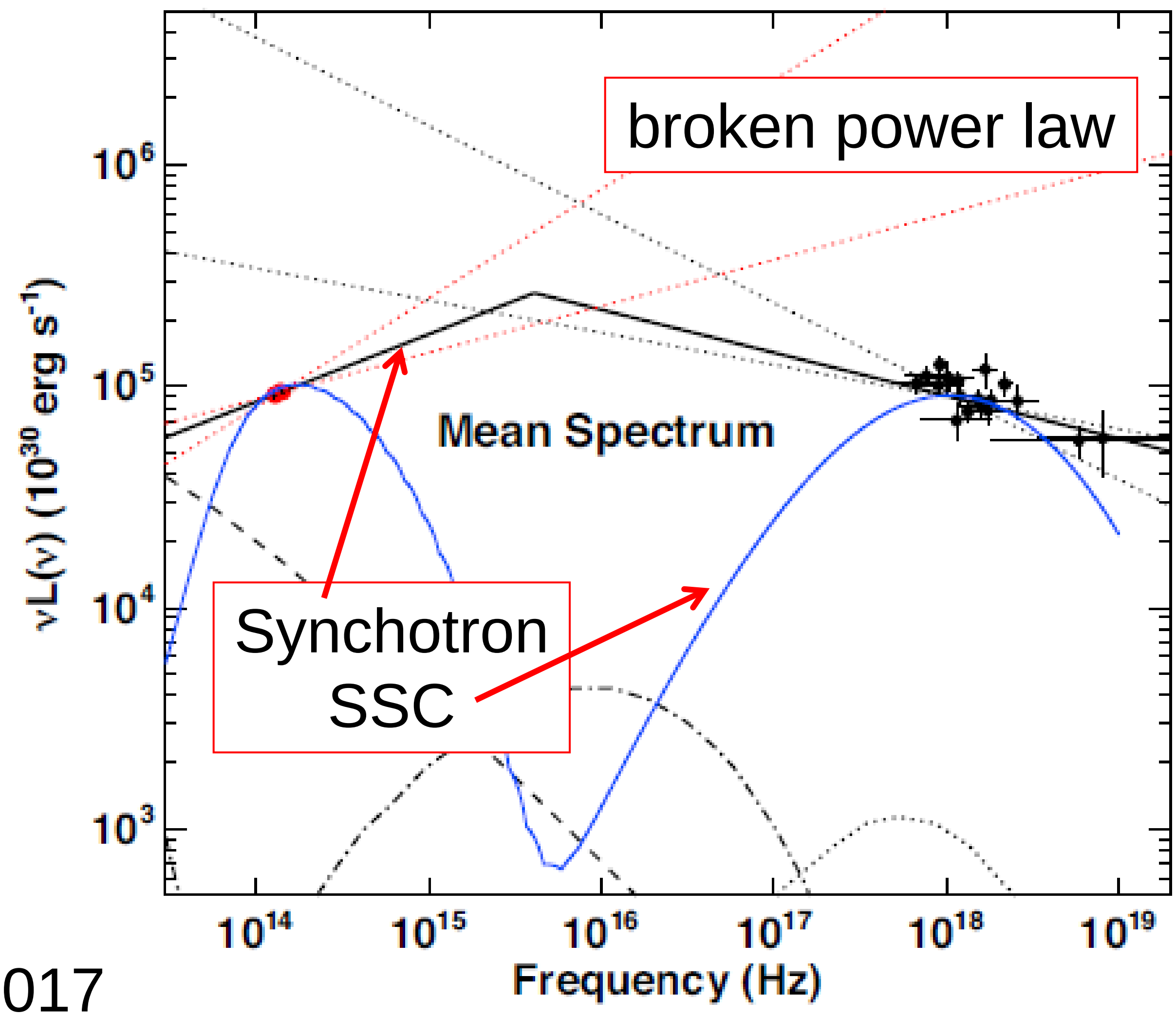

Ponti et al. 2017

Question: Where is the SSC spectrum of the broken power law?

VLBI Imaging of SgrA*

VLBI at 230 GHz (1.3 mm wavelength)

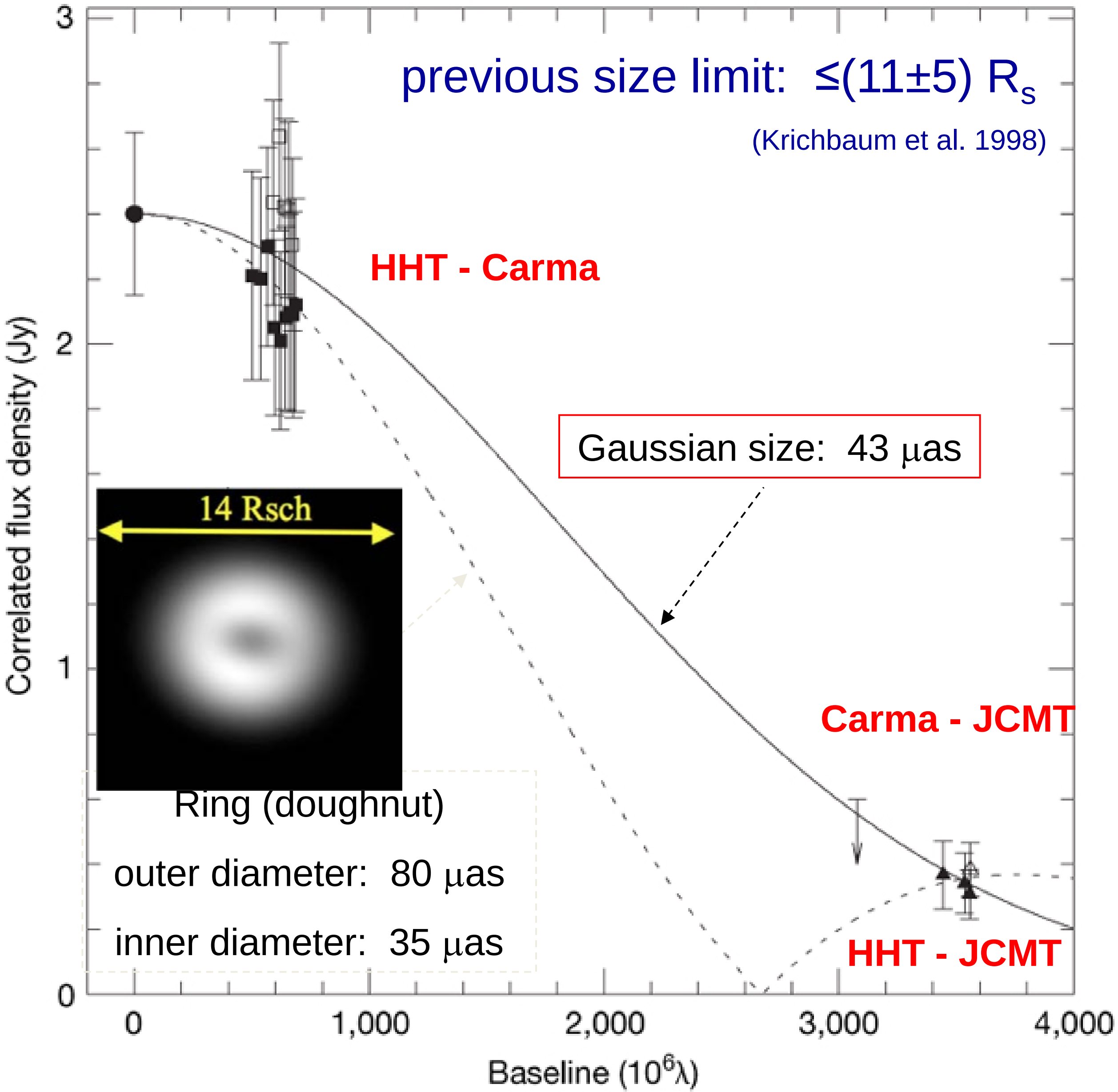

Doeleman *et al. Nature* **455**, 78-80 (2008)

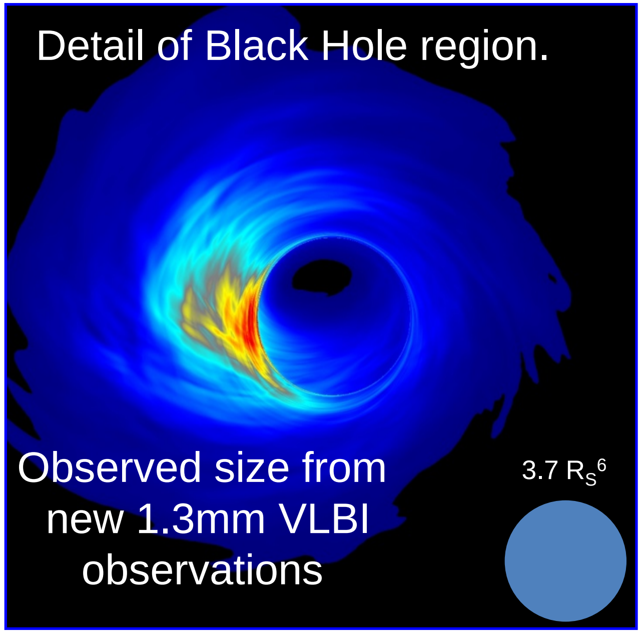

observed size:

43 (+14/-8) μas

deconvolved :

37 μas (3.7 R_S)

Intrinsic source components versus stattering speckles

The Astrophysical Journal, 824:40 (10pp), 2016 June 10

Gisela N. Ortiz-León[1] et al.

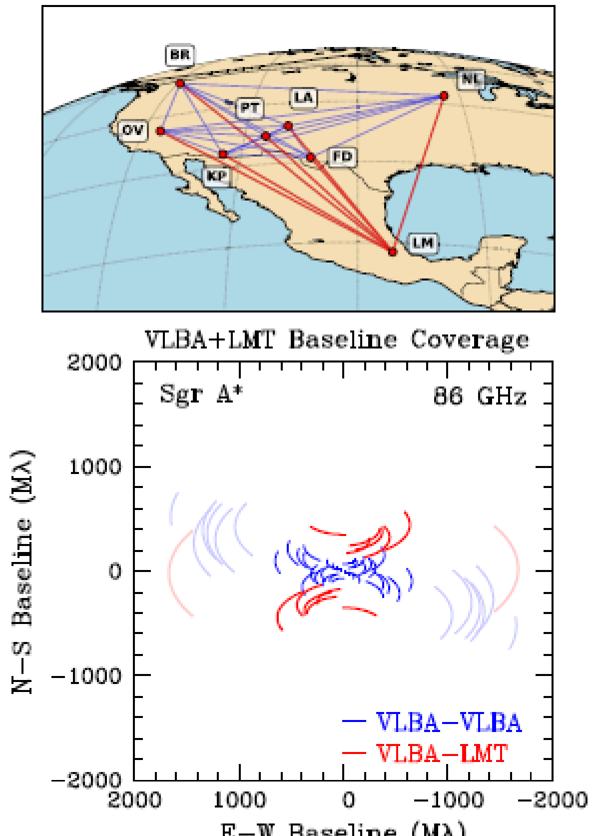

Figure 2. Top: the 3.5 mm stations of the VLBA and the LMT. Bottom: the corresponding u–v coverage; the faint tracks denote baselines to Mauna Kea, on which we do not detect Sgr A*.

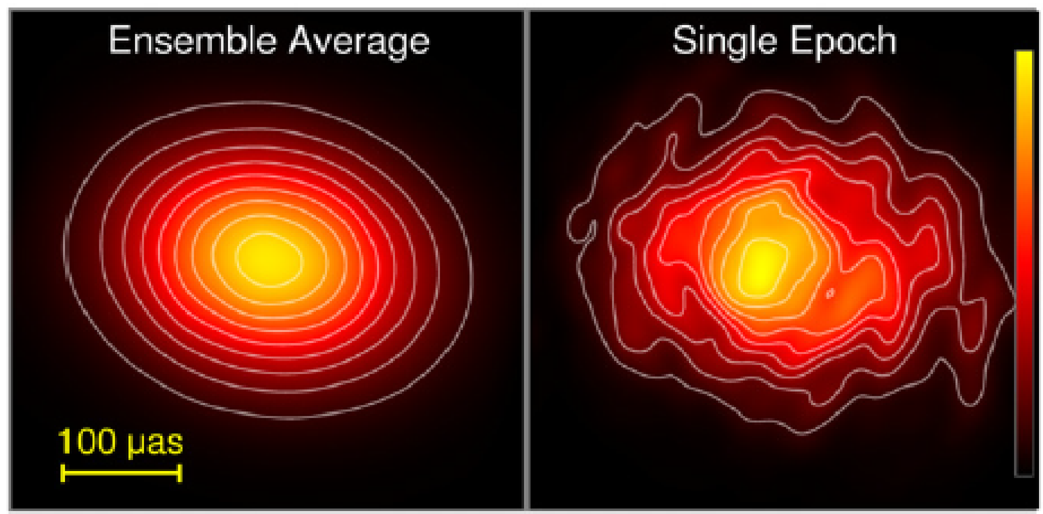

Brinkerink et al. 2016

Rauch et al. 2016

Spectral properties in the radio domain

Synchrotron Radiation

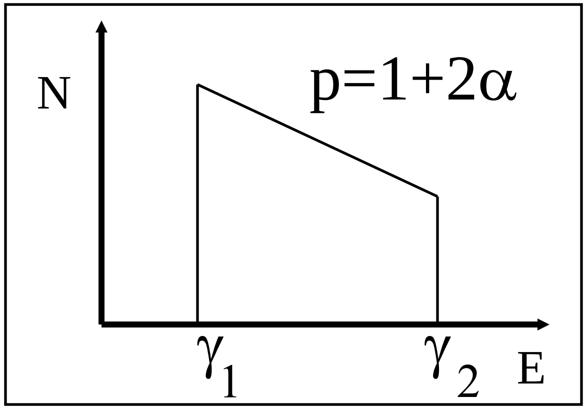

cloud of relativistic electrons threaded by tangeled magnetic field lines

relativistic electron spectrum

$$N(E) = N_0 E^{-(2\alpha+1)} (\gamma_1 mc^2 < E < \gamma_2 mc^2)$$

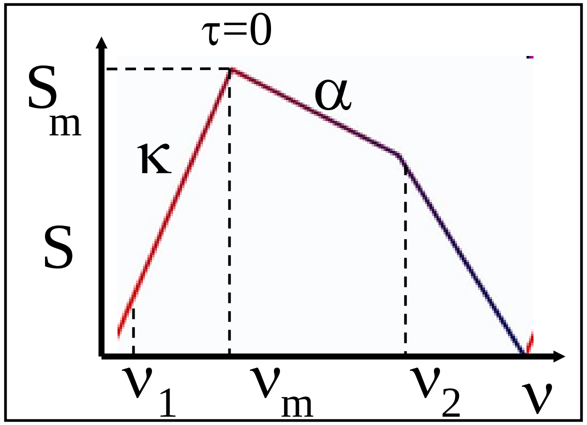

$$S_\nu \propto \nu^\alpha$$

α=-0.7
κ=+2.4

$$\boxed{B = 10^{-5} b(\alpha)\theta^4 \nu_m{}^5 S_m{}^{-2} \left(\frac{\delta}{1+z}\right) \text{gauss}}$$

DIMENSIONLESS PARAMETERS OF THE SPECTRAL INDEX α

α	b	n	d
0.25	1.8	7.9	130
0.50	3.2	0.27	43
0.75	3.6	0.012	18
1.00	3.8	0.00059	9.1

with boosting factor δ

$$\delta \; (= \Gamma^{-1}[1 - \beta \cos \phi]^{-1}$$

and bulk Lorentz factor Γ

$$\Gamma = [1 - \beta^2]^{-1/2})$$

high freq. cutoff $\nu_2 = 2.8 \times 10^6 B \gamma_2{}^2$

Synchrotron Self Compton Mechanism

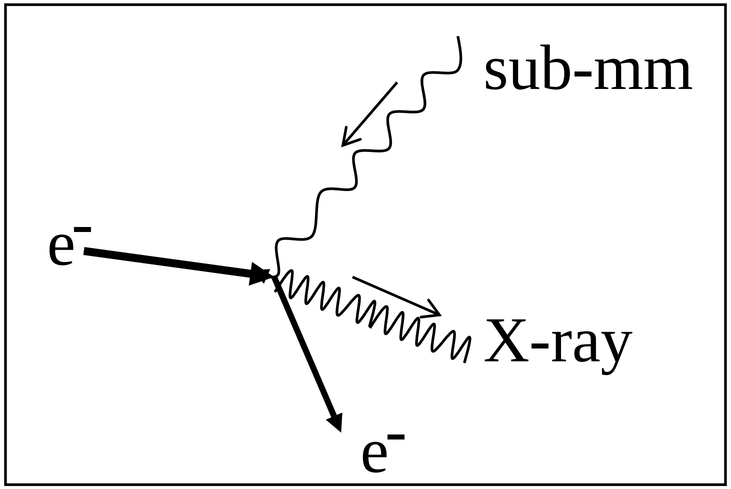

$$\gamma_e = (1-\beta_e^2)^{-1/2}$$

$$\Gamma_{bulk} = (1-\beta_{bulk}^2)^{-1/2}$$

$$\delta = \Gamma^{-1}(1-\beta_{bulk}\cos\phi)^{-1}$$

'Isotropic' velocity distribution of relativistic electrons in cloud: γ

bulk motion of the entire cloud: Γ

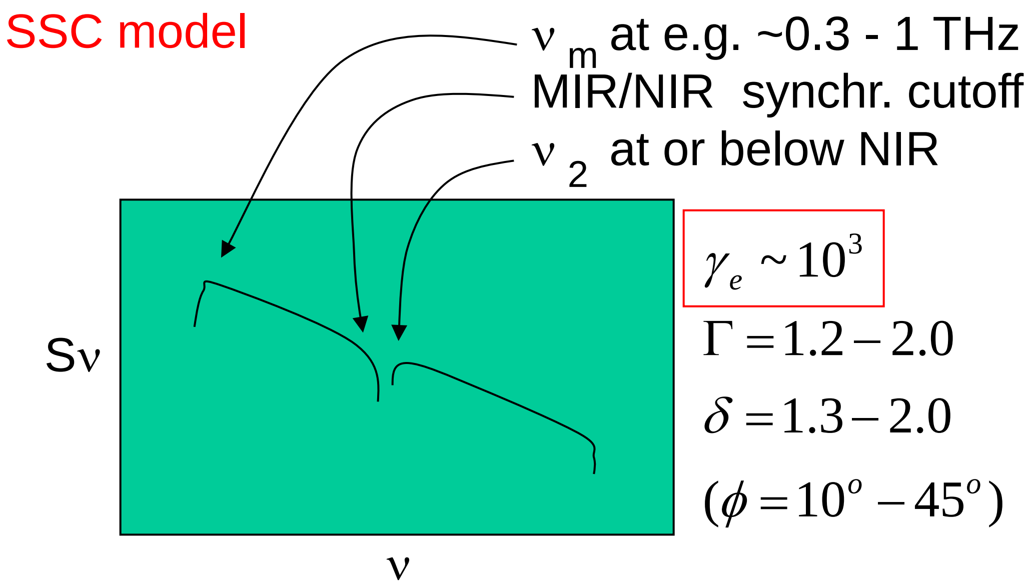

$$\gamma_e \sim 10^3$$

$$\Gamma = 1.2 - 2.0$$

$$\delta = 1.3 - 2.0$$

$$(\phi = 10^o - 45^o)$$

particle density:

$$N_0 = n(\alpha) D_{\mathrm{Gpc}}^{-1} \theta^{-(4\alpha+7)} \nu_m^{-(4\alpha+5)} S_m^{2\alpha+3} \times (1+z)^{2(\alpha+3)} \delta^{-2(\alpha+2)} .$$

Synchrotron Self-Compton

SSC flux density:

$$S_\nu^C(E_{\mathrm{keV}}) \approx d(\alpha) \ln(\nu_2/\nu_m) \theta^{-2(2\alpha+3)} \nu_m^{-(3\alpha+5)} \times S_m^{2(\alpha+2)} E_{\mathrm{keV}}^{-\alpha} [(1+z)/\delta]^{2(\alpha+2)} \ \mu\mathrm{Jy}$$

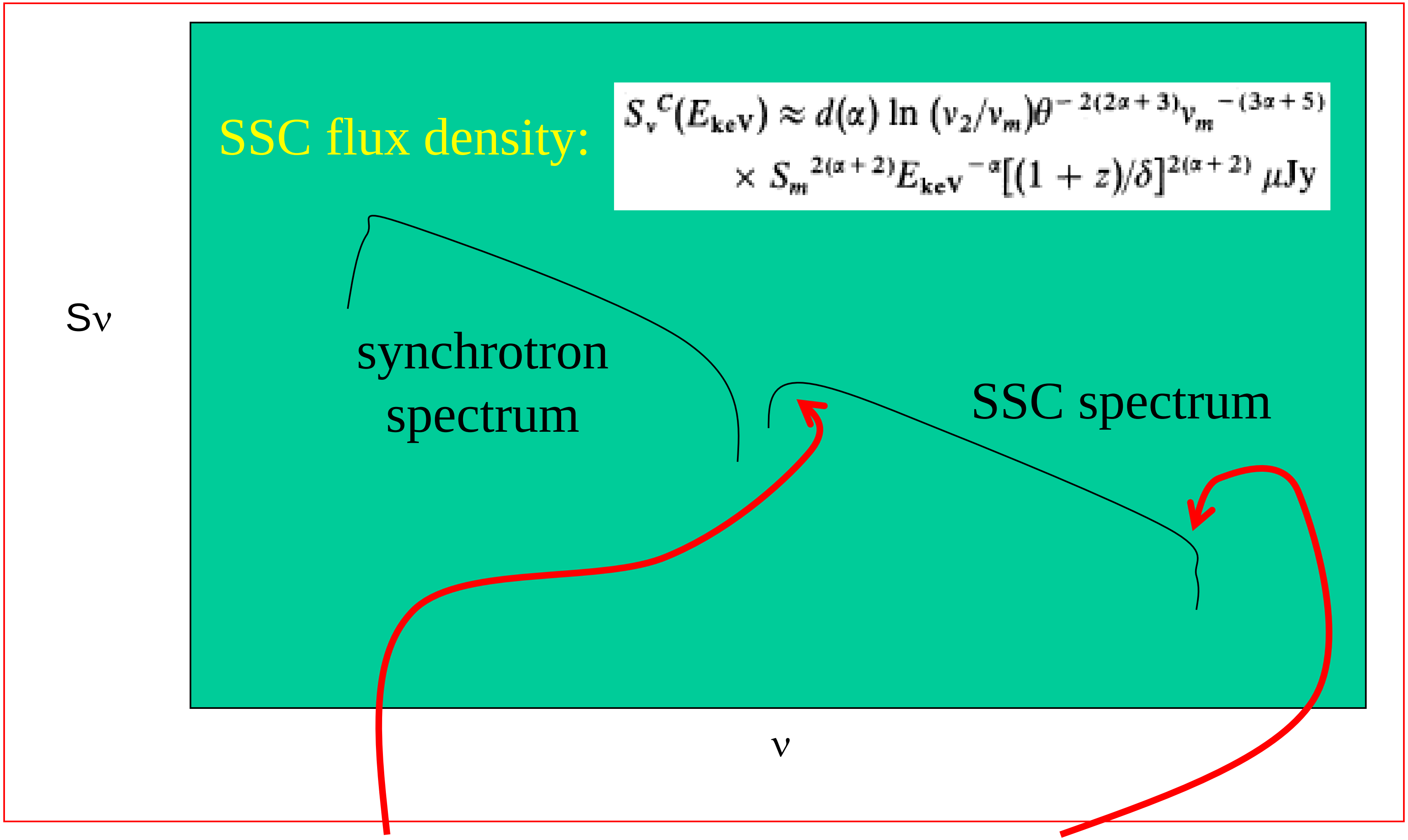

$$5.5 \times 10^{-9} \gamma_1^2 \nu_m \lesssim E_{\mathrm{keV}} \lesssim 0.2 b^{-1}(\alpha) \theta^{-4} \nu_2^2 \nu_m^{-5} S_m^2 [(1+z)/\delta]^2$$

Theory

Radiative Models of Sgr A* from GRMHD Simulations

MOTION IN
OR CLOSE TO
THE MIDPLANE

relativistic effects
may become
observable here

Accretion of matter onto SgrA* results in a variable spectrum

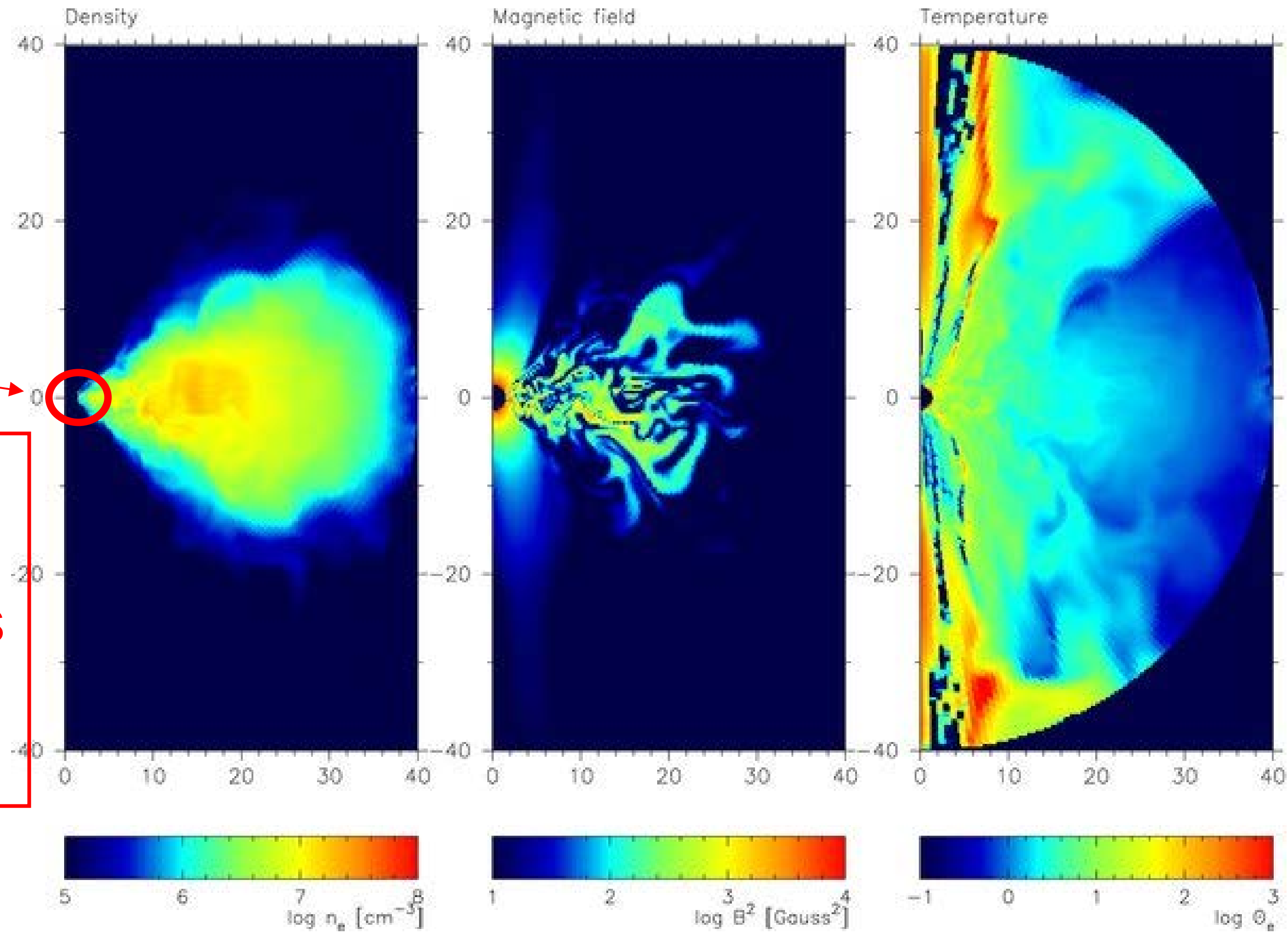

Mościbrodzka+ 2010, 2009
Dexter+ 2010

SgrA* - Stable Geometry and Accretion

SgrA* is a stable system

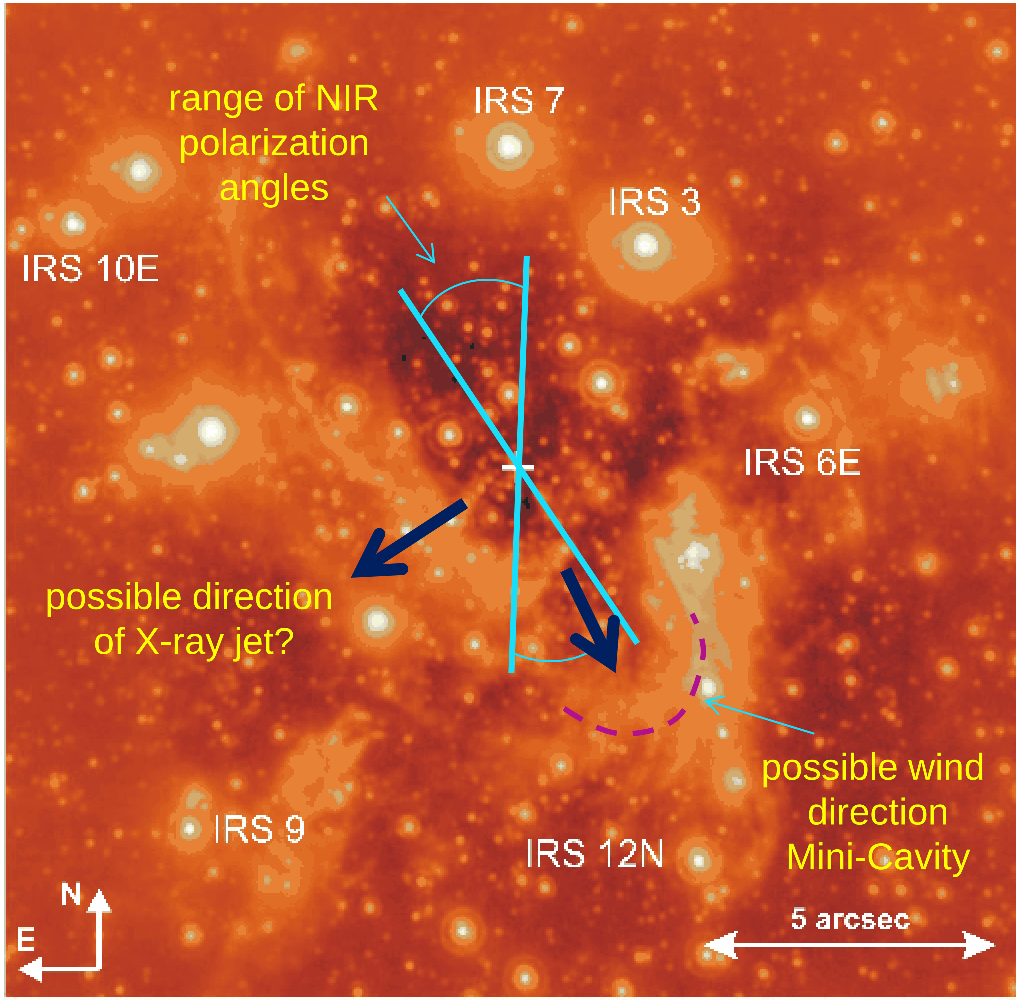

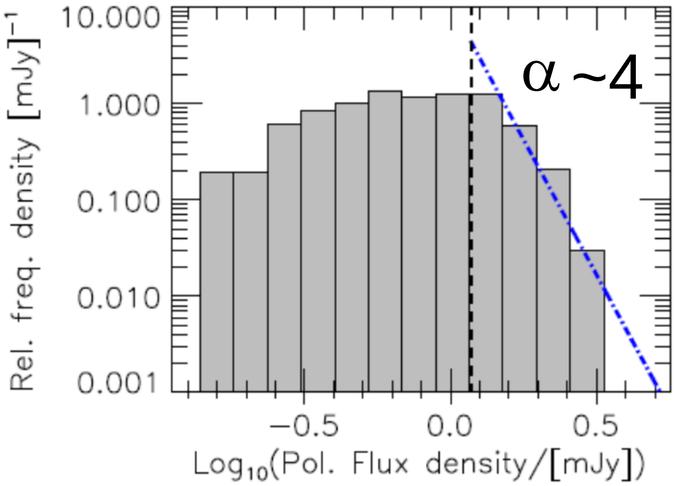

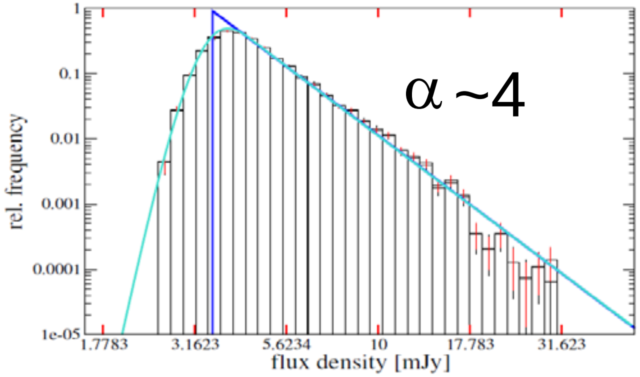

SgrA* 345GHz/100GHz varibility

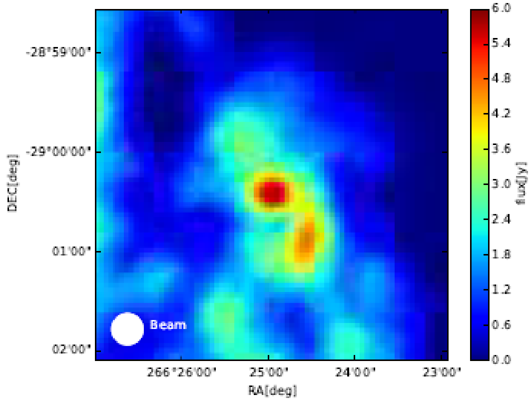

Fig. 1. A single measurement map of the GC from 2009-05-17T04:19:58, the extended submm emission from the surroundings of Sgr A* (CNR and Minispiral) dominate the data.

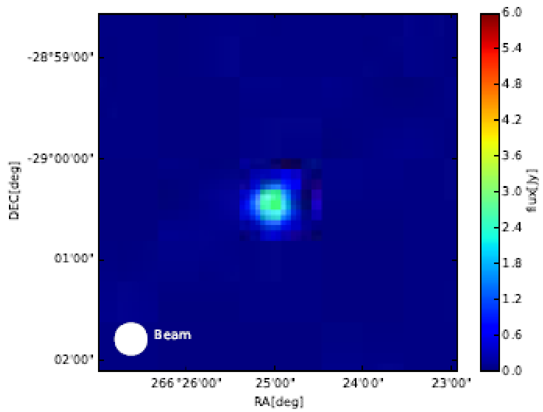

Fig. 2. A single measurement map of the GC from 2009-05-17T04:19:58 with subtracted background. The remaining point-like source represents the submm emission from Sgr A* itself.

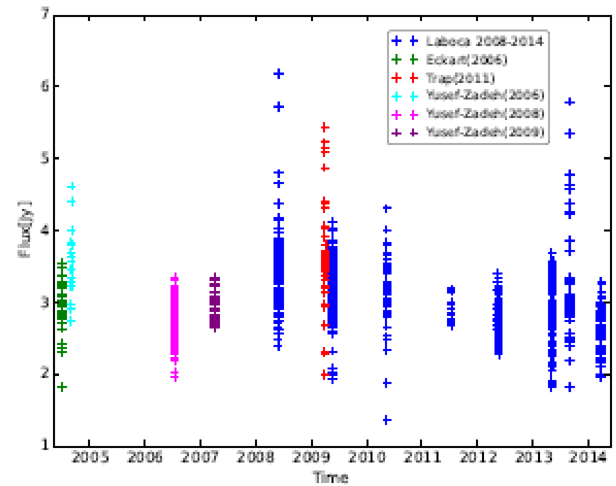

Fig. 3. All light curves obtained between 2004 and 2014. This plot contains both the LABOCA data (blue markers) and the literature data (other colors).

Borkar et al. MNRAS 2016
Subroweit et al. 2016

SgrA* 345GHz/100GHz varibility

Borkar et al. MNRAS 2016
Subroweit et al. 2016

$\alpha \sim 4$ for 100 and 345 GHz

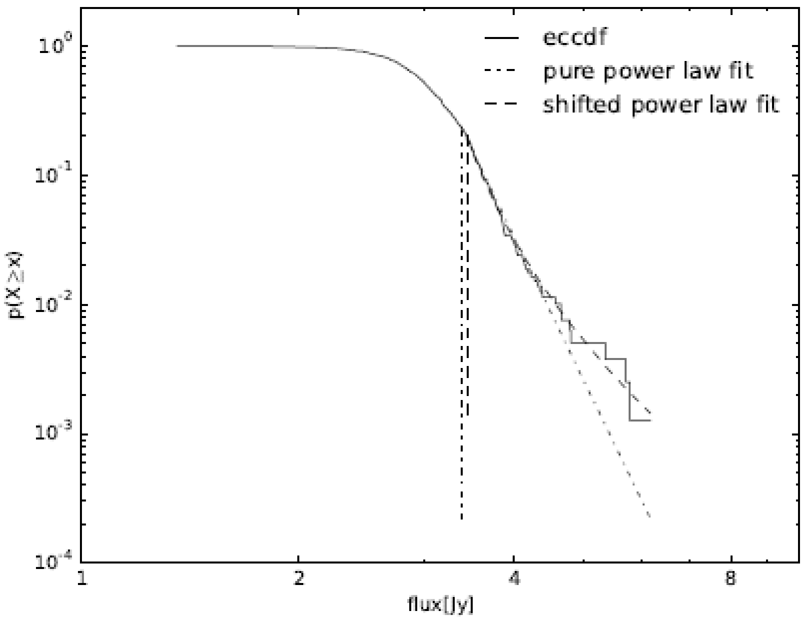

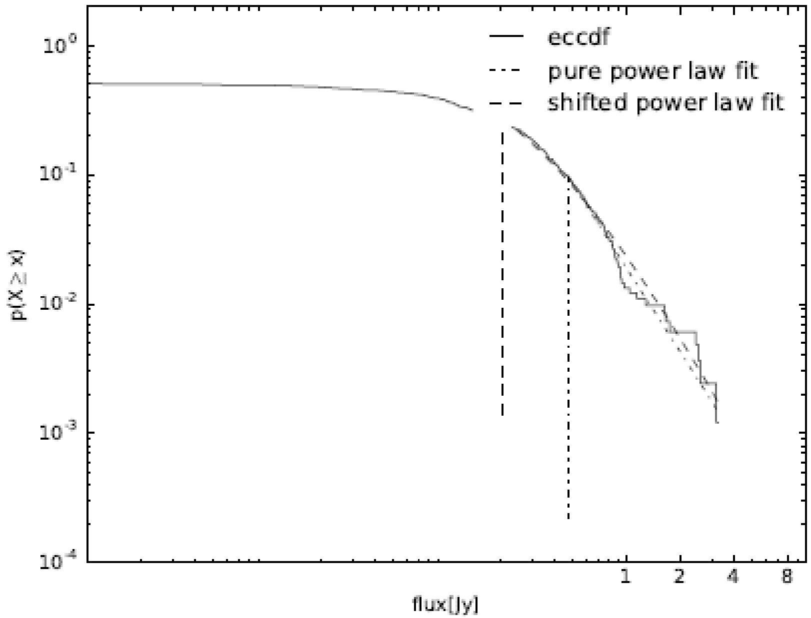

345 GHz LABOCA

100 GHz ATCA

$$S(100\ \mathrm{GHz}, t) \sim S(\nu_0 = 100\ \mathrm{GHz}, t) + S_{\mathrm{adiab}}(\nu_0 > 100\ \mathrm{GHz}, t)$$

Adiabatic Expansion in SgrA*

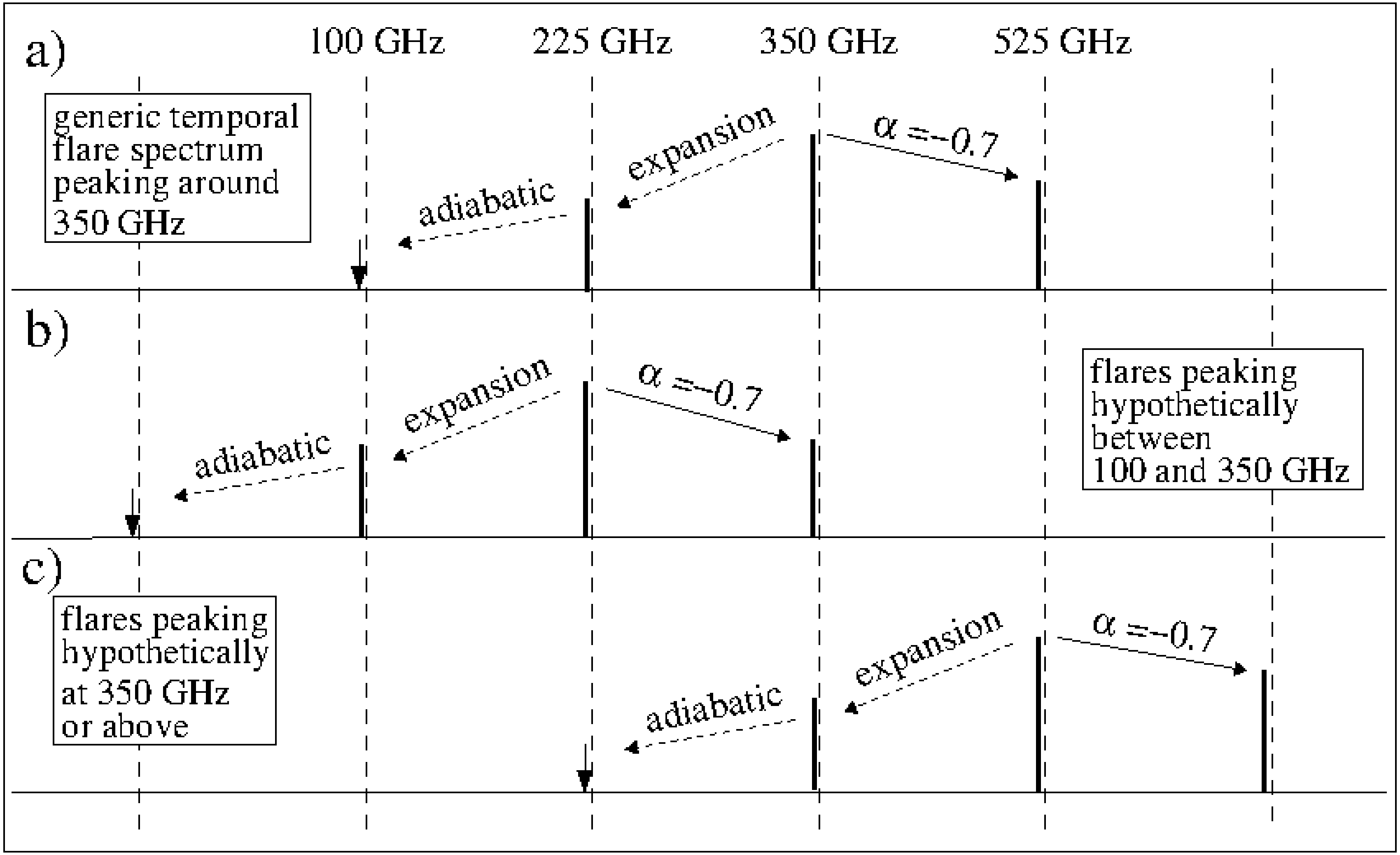

Subroweit et al. 2016

Adiabatic Expansion in SgrA*

$$\nu_{\rm m} = \nu_{\rm m0}\left(\frac{R(t)}{R_0}\right)^{-(4p+6)/(p+4)}$$

van der Laan (1966)

$$p = 1 - 2\alpha_{\rm sync} \sim 2.4,$$

$$\frac{R(t)}{R_0} \sim \left(\frac{\nu_{\rm m}}{\nu_{\rm m0}}\right)^{-1/2.44} \sim \left(\frac{100\,\rm GHz}{350\,\rm GHz}\right)^{-1/2.44} \approx 1.67$$

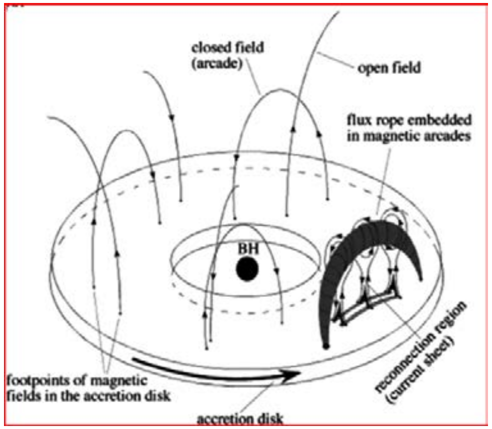

Yuan et al. 2009

$$R(t) = v_{\rm exp}t + R_0$$

starting at ~1 Rs

$$v_{\rm exp} \times 0.5\,\rm h \sim 0.67\,R_S.$$

$$\boxed{v_{\rm exp} \sim 0.01\,\rm c}$$

Subroweit et al. 2016

Synchrotron Modeling

Rapid variability time scales (< 1hour) imply
a non-thermal radiation mechanism:

$$S_{X,ssc} = d(\alpha)\ln\left(\frac{\nu_2}{\nu_m}\right)\theta^{-2(2\alpha+3)}\nu_m^{-(3\alpha+5)}S_m^{2(\alpha+2)}E_X^{-\alpha}\delta^{-2(\alpha+2)},$$

$$B = 10^{-5}b(\alpha)\theta^4\nu_m^5 S_m^{-2}\delta,$$

$$N_0 = n(\alpha)D_{Gpc}^{-1}\theta^{-(4\alpha+7)}\nu_m^{-(4\alpha+5)}S_m^{2\alpha+3}\delta^{-2(\alpha+2)},$$

Marscher 1983, 2009

Visualization of possible flare scenarii

Possible flare models

NIR X-ray

SYN-SYN: Synchrotron-synchrotron

SYN-SSC: Synchrotron-Self-Compton

SSC-SSC: Self-Compton-self-Compton

Eckart et al. 2012

Parametrization of the logarithmic expression

Two extreme cases:
High demands on electron acceleration or density

SYN-SYN: X-ray produced by synchrotron radiation;
<10% by SSC

SSC-SSC: X-ray produced by synchrotron self-Compton;
<10% by SYN; required density higher than average

Moderate demand on density and acceleration

SYN-SSC: radio/NIR by Syncrotron and X-ray by SSC

Eckart et al. 2012

Visualization of possible flare scenarii

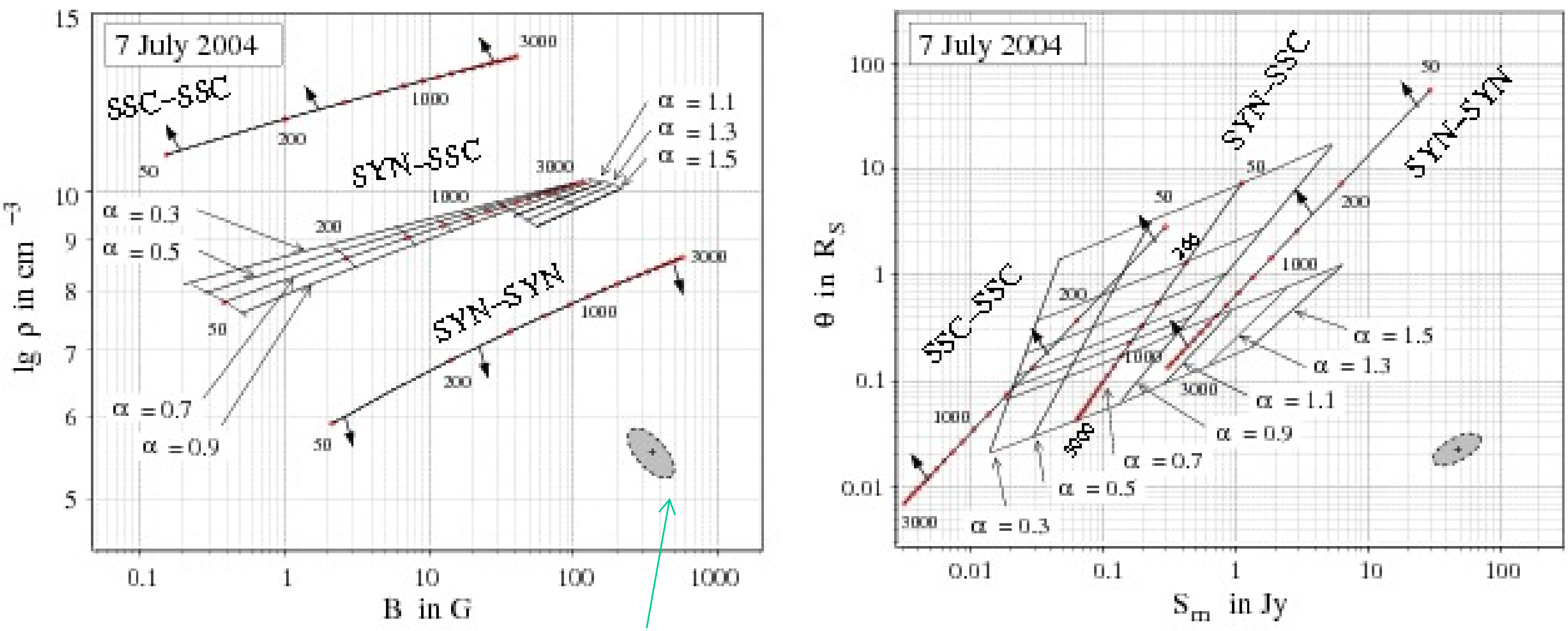

parameterized by case spectral index and turnover frequency νm.

Uncertainties due to measurement uncertaintuies

Solutions obey MIR flux limits (Schödel+ 2010,11) and: If SYN dominates - then less than 10% of the radiation should be due to SSC and vice versa.

Arrows point into directions of even more stringent constrains.

Eckart et al. 2012

Variability in the SYN-SSC case

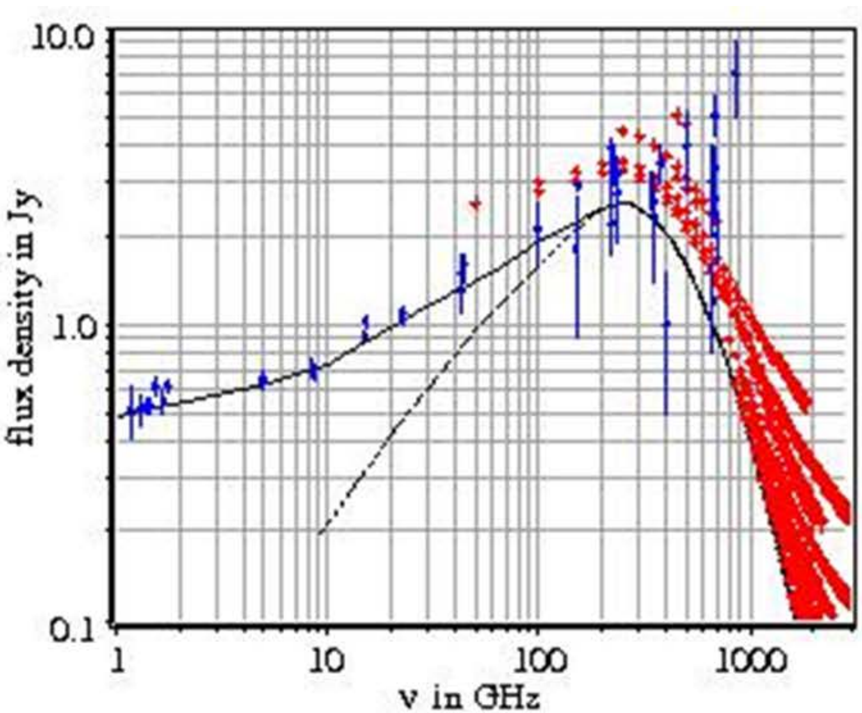

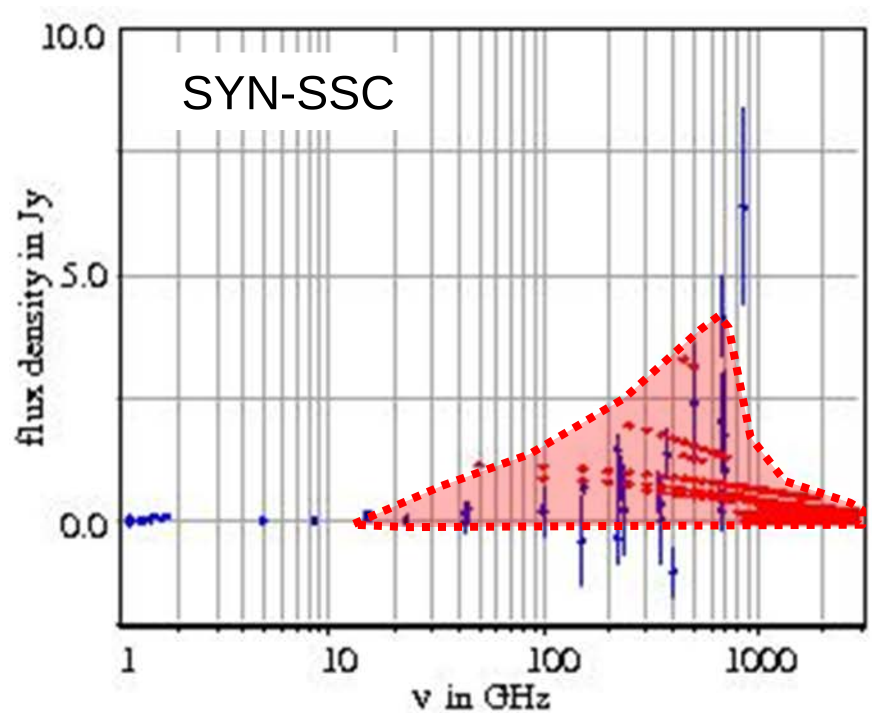

SYN-SSC: Density moderate - consistent with MHD model of mid-plane. Moderate demand on electron acceleration.

Eckart et al. 2012

Spectral properties in the X-ray domain
Statistics of NIR/X-ray light curves of SgrA*

Synchrotron radiation is responsible for flux density variations in the NIR – which can be studied there best – without confusion due to fluxes from the larger scale accretion stream.

Flux density histogram for SgrA*

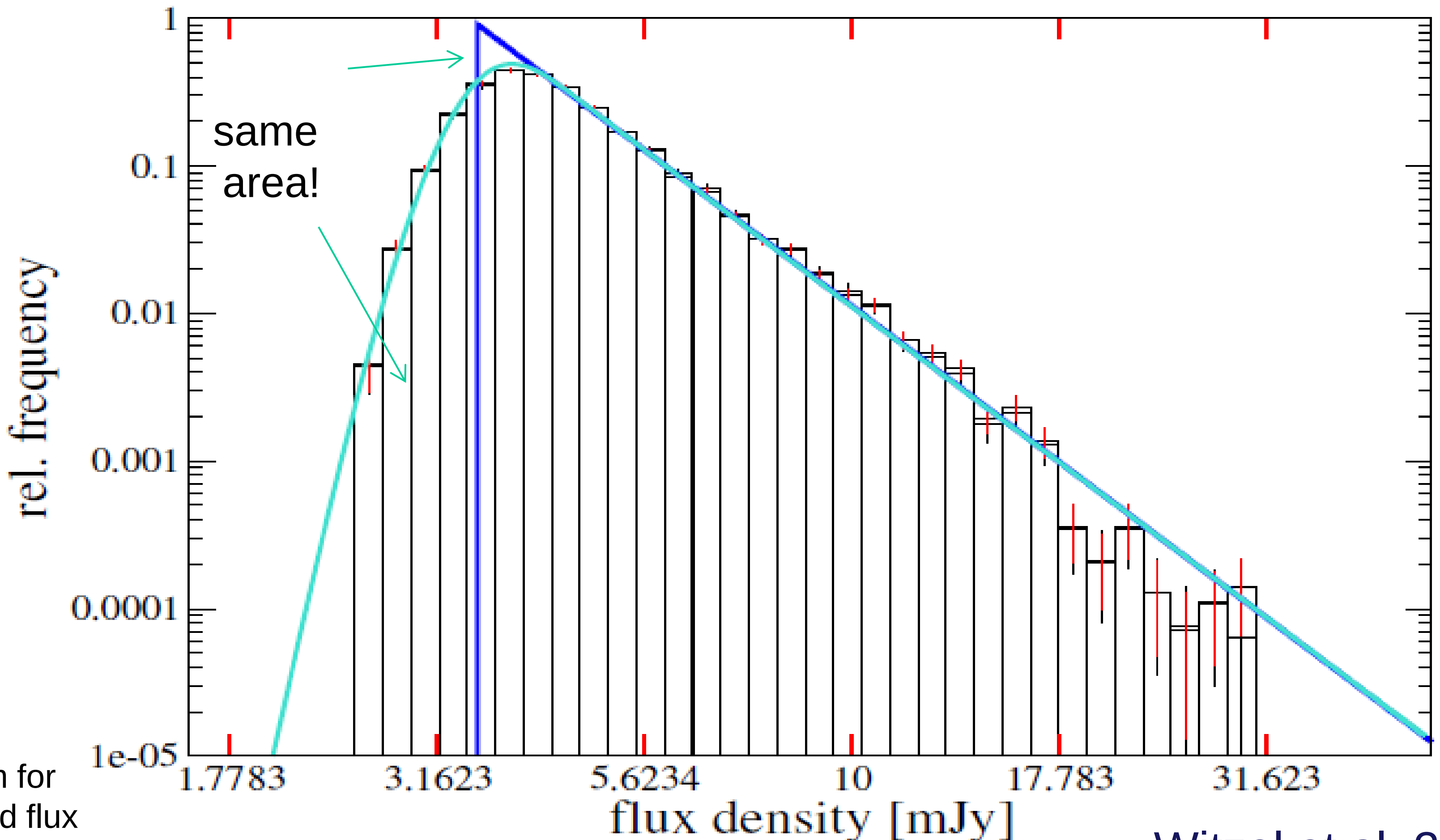

Diagram for polarized flux in work

Witzel et al. 2012

The brown line shows the extrapolation of the best power-law fit, the cyan line the power-law convolved with a Gaussian distribution with 0.32 mJy width.

X-ray light echo : variability of SgrA*

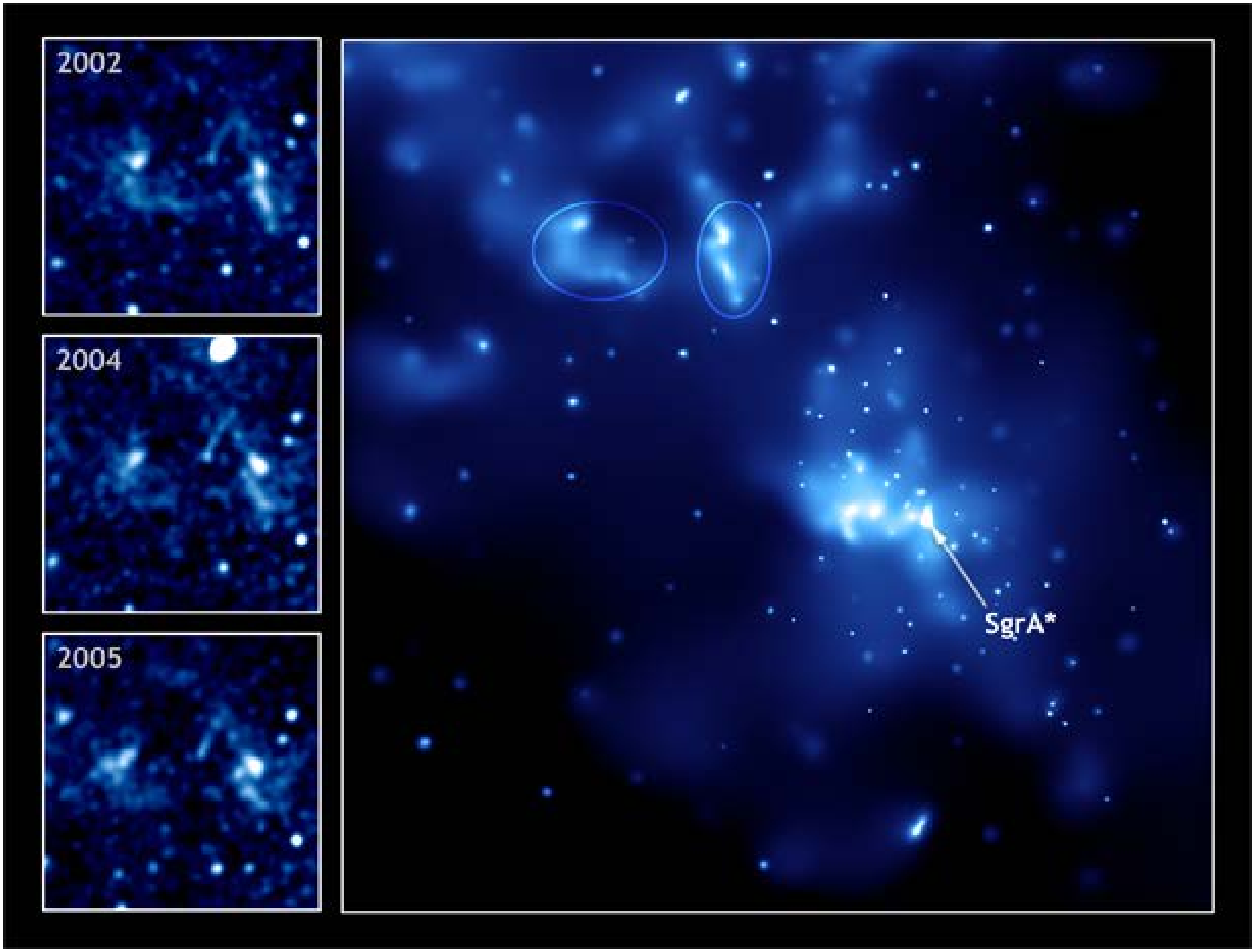

Chandra/ NASA

The statistics allows to explain the event 400 years ago that results in the observed X-ray light echo

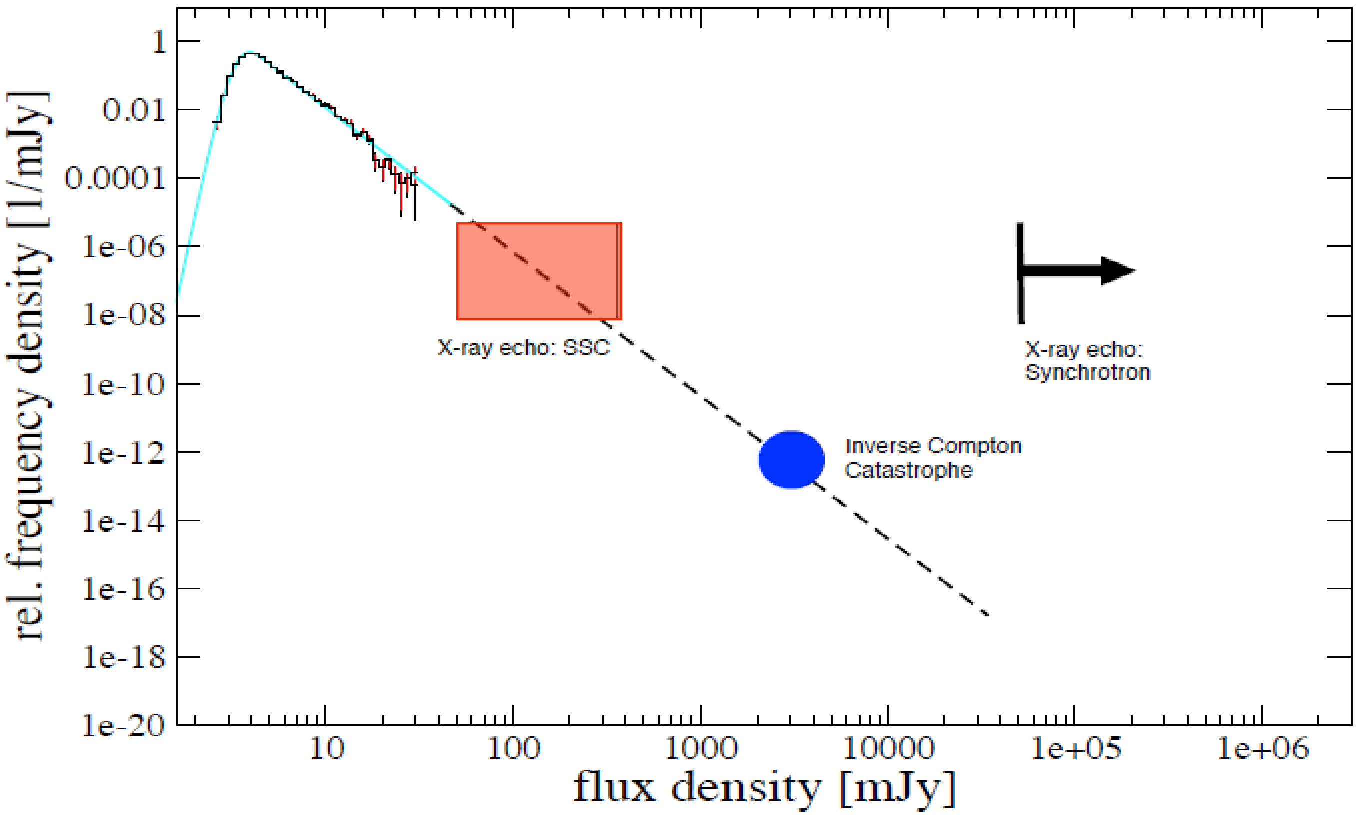

Fluorescent back-scatter from molecular clouds surrounding the GC:

Revnivtsev et al. 2004,
Sunyaev & Churazov 1998,
Terrier et al. 2010

and

Witzel et al. 2012

Illustration of a flux density histogram extrapolated from the statistics of the observed variability. The expected maximum flux density given by the inverse Compton catastrophe and a estimation of its uncertainty is shown
as the magenta circle, the SSC infrared flux density for a bright X-ray outburst as expected from the observed X-ray echo is depicted as the red rectangular.

Spectral properties in the X-Ray domain

Chandra X-ray flare statistics in the 2-8 keV band

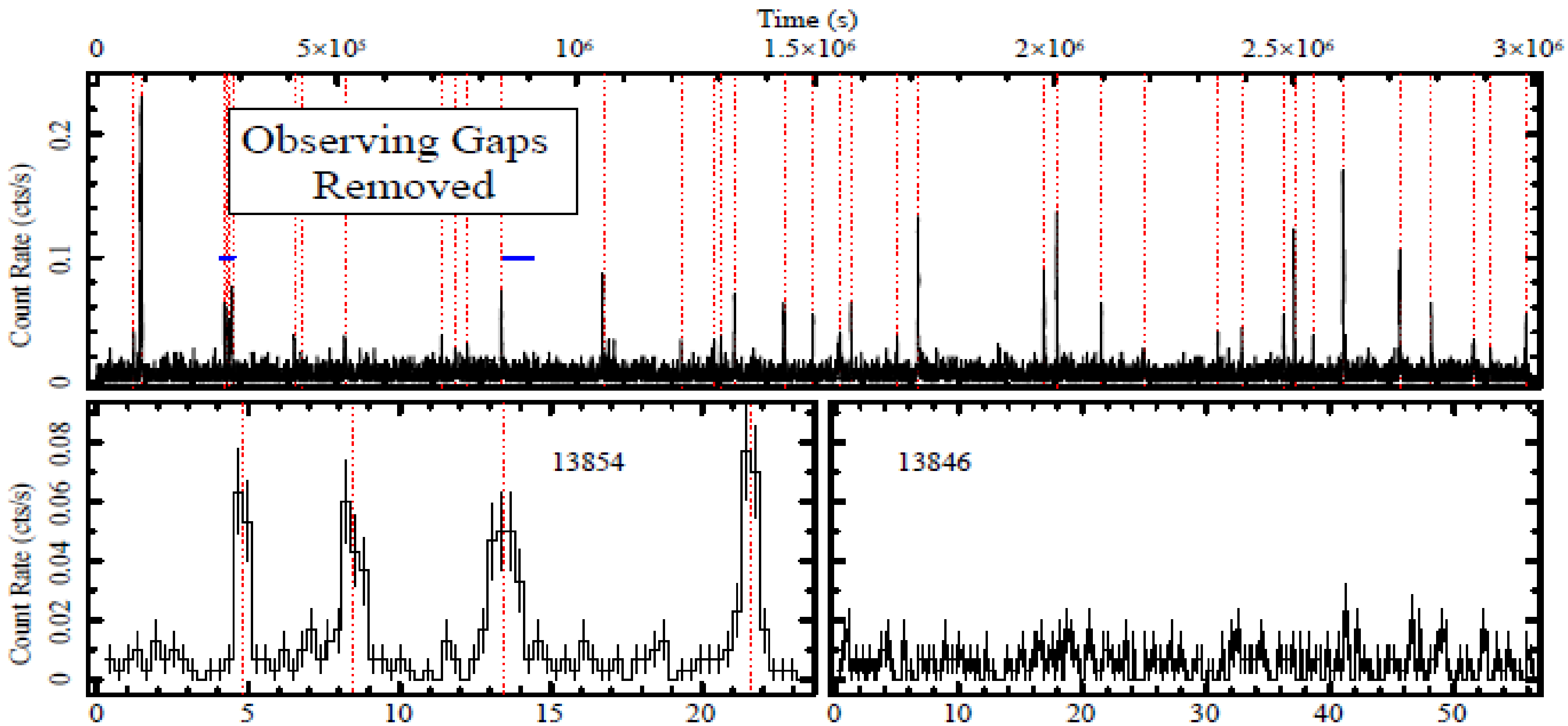

Neilsen, Novak et al. 2013: 39 detected flares in the 3Ms X-ray Visionary Project (XVP) observations. **Mean X-ray flare rate: ~1 per day; (NIR ~4/day);** mean X-ray flare luminosity 5x10^34 erg/s (10 times fainter than the brightest Chandra flare; Novak et al. 2012); up to Γ=2; dN/dL~L^(-1.9+-0.4)

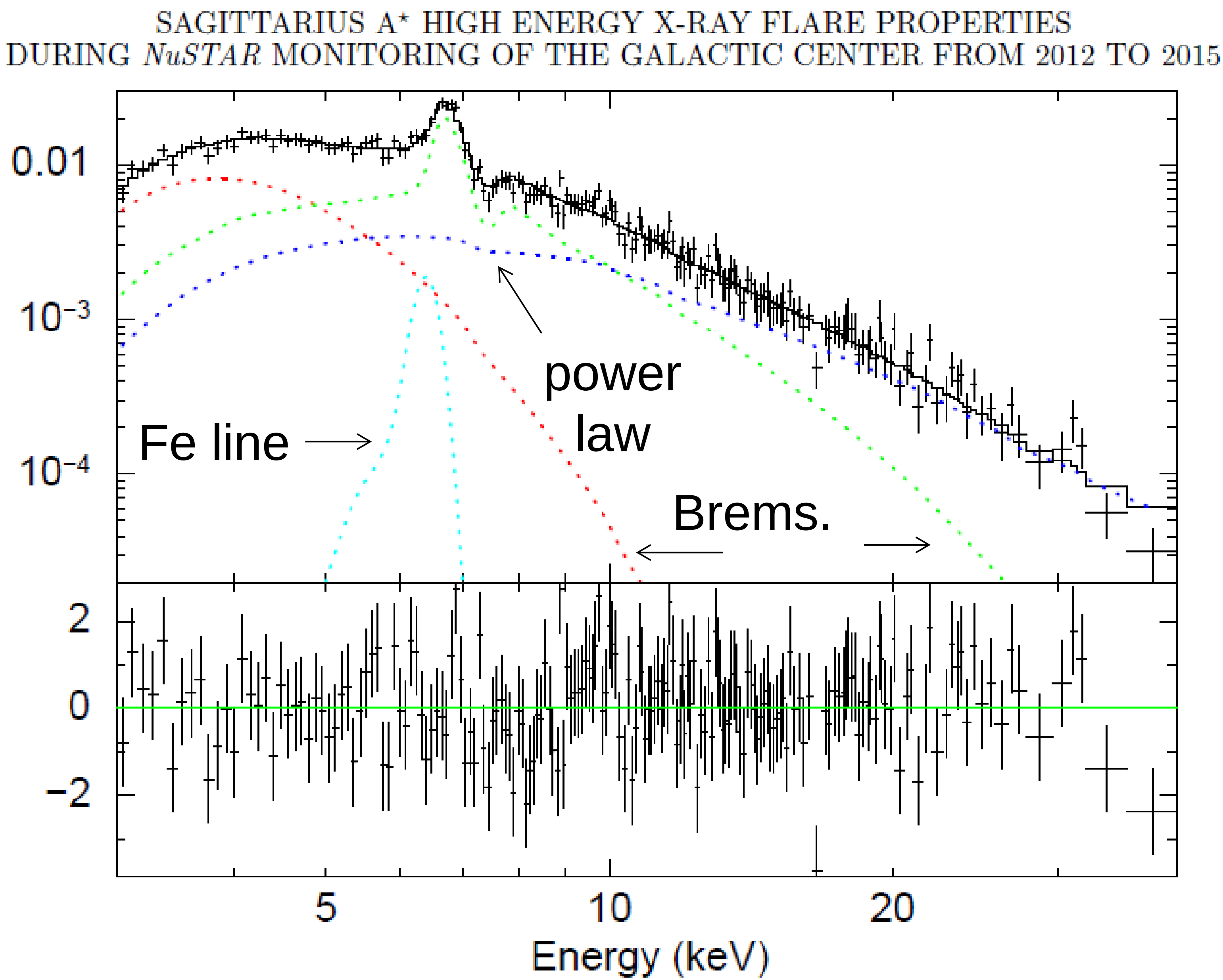

Shuo Zhang et al. ApJ 2017

Co-addition of brightest **NuSTAR** flares

SAGITTARIUS A* HIGH ENERGY X-RAY FLARE PROPERTIES
DURING *NuSTAR* MONITORING OF THE GALACTIC CENTER FROM 2012 TO 2015

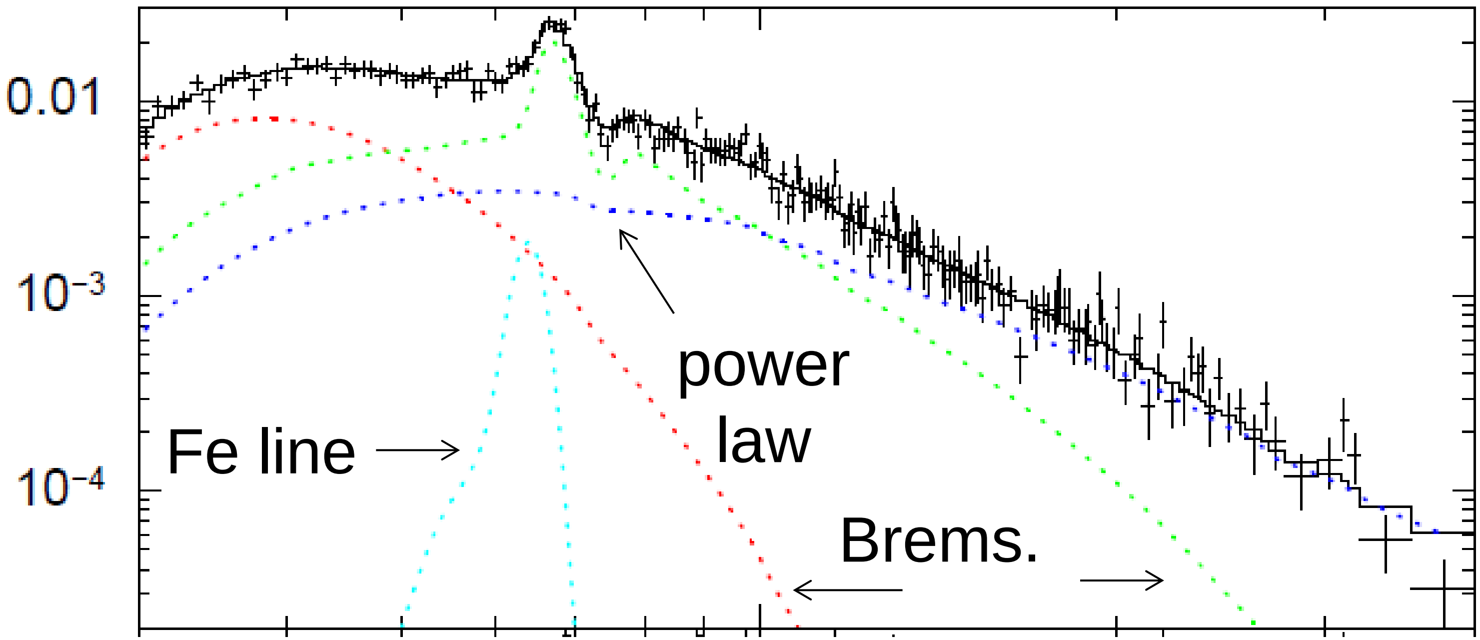

Synchrotron versus SSC

No spectral breaks – but: The case is not conclusive yet: bright SSC spectrum will cover the entire spectral range as well - with the same spectral index!

Shuo Zhang et al. ApJ 2017

Summary

- SgrA* as a Low Luminosity (aktive) Source
  yes

- Radio domain: Variability / spectral index
inverted, highly variable, clear indications of adiabatic expansion, most bright flares originate in the 300-400 GHz sub-millimeter domain

- Mid/Near-infrared domain
optically thin synchrotron radiation, highly variable, no detectable low state

- X-Ray domain
strong flare activity, some flares may be pure synchrotron flare, it is, however, easier to produce adequate SSC flux

End